

J. A. D. Connolly

Phase diagram methods for graphitic rocks and application to the system C–O–H–FeO–TiO₂–SiO₂

Received: 13 December 1993 / Accepted: 4 July 1994

Abstract Carbon-saturated C–O–H (GCOH) fluids have only one compositional degree of freedom. This degree of freedom is specified by the variable X_O that expresses the atomic fraction of oxygen relative to oxygen + hydrogen. The only valid constraint on the maximum in the activity of GCOH fluid species is related to the bulk composition of the fluid, as can be expressed by X_O . In fluid-saturated graphitic rocks, mineral devolatilization reactions are the dominant factor in determining the redox state of the metamorphic environment. X_O is directly proportional to the f_{O_2} of GCOH fluid, and because its value can only be affected by fluid-rock interaction, it is an ideal measure of the redox character and composition of GCOH fluid. Phase diagrams as a function of X_O are analogous to the P – T – X_{CO_2} diagrams used for binary H₂O–CO₂ fluids; this analogy can be made rigorously if the C–O–H fluid composition is projected through carbon into the O–H subcomposition. After projection, the fluid is described as a binary fluid with the components O and H, and the compositional variable X_O . Description of GCOH fluids in this manner facilitates construction of phase diagram projections that define the P – T stability of mineral assemblages for all possible fluid compositions as well as fluid-absent conditions. In comparison to phase diagrams with variables based on the properties of fluid species, P – T – X_O diagrams more clearly constraint accessible fluid compositions and fluid evolution paths. Calculated P – T – X_O projections are presented for the C–O–H–FeO–TiO₂–SiO₂ system, a limiting model for the stability of Fe–Ti oxides in graphitic metapelites and phase relations in metamorphosed iron-formations.

With regard to the latter, the stability of the assemblage qtz + mag + gph has been a source of controversy. Both the calculated C–O–H–FeO–TiO₂–SiO₂ system petrogenetic grid and natural examples, suggest that this assemblage has a large P – T stability field. Discrepancies between earlier C–O–H–FeO–SiO₂ system phase diagram topologies are reconciled by the qtz + mag + gph = sid + fa phase field, a barometric indicator for metamorphosed-iron formations. A more general implication of calculated P – T – X_O phase relation is that few inorganic mineral-fluid equilibria appear to be capable of generating hydrogen-rich, $X_O < \frac{1}{3}$, GCOH fluids at crustal metamorphic conditions. The utility of P – T – X_O diagrams derives from the use of a true compositional variable to describe fluid composition, this approach can be extended to the treatment of carbon-undersaturated systems, and provides a simple means of understanding metasomatic processes of graphite precipitation.

Introduction

Phase equilibria between minerals and C–O–H fluid are conventionally characterized by pressure, temperature and properties related to the concentration or thermodynamic activity of fluid species (e.g., f_{O_2} , a_{H_2O} , or γ_{CO_2} , see Table 1 for notation). A drawback of employing these properties is that they depend both on homogeneous equilibria within the fluid, and thus on pressure and temperature, and on processes of mineral-fluid interaction. For example, if the f_{O_2} of two different geologic environments is known, it is not possible to establish which environment is more oxidizing without first determining the effect on f_{O_2} of changing pressure and temperature between the two environments when no fluid-rock interaction occurs. Moreover, variables based on properties of a fluid species have little absolute significance because the possible range of the variables cannot be defined independently of

J. A. D. Connolly
Institute for Mineralogy and Petrography,
Swiss Federal Institute of Technology, CH-8092 Zürich,
Switzerland

Editorial responsibility: J. Hoefs

Table 1 Frequently used symbols and phase notations

Symbol	Meaning
a_i	activity of entity i , relative to a pure standard state
f_i	fugacity of entity i , relative to a 1 bar, pure, ideal gas standard state
G_i°	standard state molar Gibbs energy of entity i
G_i	partial molar Gibbs energy of entity i
n_i	number of moles of entity i
P	pressure
T	temperature
X_{CO_2}	mole fraction of CO_2 in binary $\text{H}_2\text{O}-\text{CO}_2$ fluid
X_{O}	atomic fraction of oxygen relative to oxygen + hydrogen, Eq. 1
y_i	mole fraction of species i in C-O-H fluid
Y_i	atomic fraction of component i in C-O-H fluid
Z_i	mole fraction of component i in C-O-H fluid
μ_i	chemical potential of component i
ν_i	signed stoichiometric coefficient of entity i in a reaction or phase

Phase	
fa	stoichiometric fayalite Fe_2SiO_4
fs	stoichiometric ferrosilite FeSiO_3
gph	stoichiometric graphite C
gru	stoichiometric grunerite $\text{Fe}_7\text{Si}_8\text{O}_{22}(\text{OH})_2$
hem	stoichiometric hematite Fe_2O_3
ilm	stoichiometric ilmenite FeTiO_3
mag	stoichiometric magnetite Fe_3O_4
qtz	stoichiometric quartz SiO_2
ru	stoichiometric rutile TiO_2
sid	stoichiometric siderite FeCO_3
usp	stoichiometric ulvoespinel FeTi_2O_4
F_x	C-O-H fluid; when given, x is X_{O} (mol%)
Ilm_x	Ilmenite a solution between ilm and hem; when given x is mol% ilm
Mag_x	Magnetite a solution between mag and usp; when given x is mol% mag

environmental conditions. The intent of this paper is to demonstrate that these problems are circumvented if the fluid is described by variables related to proportions of its components rather than its species. The advantage of such variables is that they are independent of processes of internal equilibration, and thus directly reflect mass balance constraints imposed on fluid-rock interaction. In the specific case of carbon-saturated systems, thermodynamic projection through carbon permits characterization of C-O-H fluid by a single binary compositional variable, X_{O} , a variable used by Labotka (1991) to describe fluid speciation. Through this transformation it becomes apparent that $P-T-X_{\text{O}}$ diagrams are exactly analogous to the $P-T-X_{\text{CO}_2}$ diagrams familiar to petrologists. However, $P-T-X_{\text{O}}$ diagrams have the advantage that they can be used to portray redox equilibria in addition to simple decarbonation and dehydration equilibria. The value of this type of approach was recognized earlier by Burt (1972), but Burt's method appears to have been overlooked by subsequent workers, possibly because Burt's

treatment was primarily topological. Many high grade graphitic rocks are thought to equilibrate in the absence of fluid (e.g., Edwards and Essene 1988; Skippen and Marshall 1991); for this situation, among others, it is useful to define both fluid saturated and under-saturated equilibria as a function of pressure and temperature, i.e., by constructing $P-T$ phase diagram projections. The interpretation and construction of such projections is shown to be straightforward and demonstrated for the system C-O-H-FeO-TiO₂-SiO₂, a model relevant to the analysis of phase relations in metamorphosed iron-formations and metapelites.

The fluid composition variable X_{O}

For a compositional variable to be of greatest meaning it must be independent of environmentally determined parameters such as pressure and temperature. In equilibrium carbon-saturated C-O-H (GCOH) fluids this is not true for any variable related to the carbon-content of the fluid, because the carbon-content must vary as a function of pressure and temperature to maintain the equality $\mu_{\text{C}} = G_{\text{graphite}}^\circ$. Thus optimal compositional variables for GCOH fluids must be related to the atomic proportions of hydrogen and oxygen in the fluid. For numerical purposes it is convenient to express these proportions by the variable:

$$X_{\text{O}} \equiv \frac{n_{\text{O}}}{n_{\text{O}} + n_{\text{H}}} \quad (1)$$

The significance of X_{O} is demonstrated by the isobaric-isothermal C-O-H phase diagram (Fig. 1). The possible compositions of a C-O-H fluid that coexists with graphite correspond to the boundary between the two-phase field in which graphite coexists with fluid and the one-phase field for carbon-under-saturated fluids. The boundary between these fields is

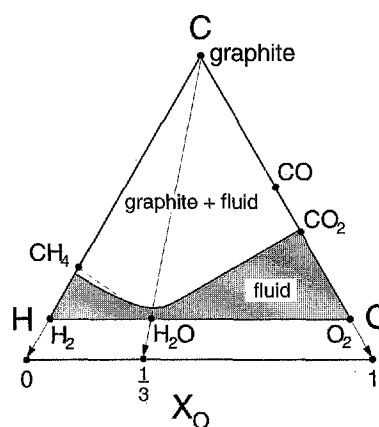


Fig. 1 Schematic isobaric-isothermal composition phase diagram for the C-O-H system illustrating the relation between X_{O} and GCOH fluid composition

the carbon-saturation surface. The composition of a C–O–H fluid that coexists with graphite (i.e., a GCOH fluid) corresponds to the point on the carbon-saturation surface intersected by a line drawn from the graphite composition through the bulk composition of the system.

For simple dehydration reactions in the presence of graphite, the fluid-forming reaction is essentially a reaction between water and graphite; thus, the fluid must have the same X_O as water, i.e., $\frac{1}{3}$ (Labotka 1991). Subsequent to its generation, the amount of carbon in the fluid varies with pressure and temperature to maintain equilibrium with graphite, but in the absence of additional fluid-rock interaction, or the introduction of externally derived H- or O-rich fluids, X_O remains constant. Connolly and Cesare (1993) argued that such perturbations are unlikely to be significant in dehydration dominated systems, such as metapelitic environments, and that in these systems an $X_O = \frac{1}{3}$ model provides a good working hypothesis for fluid composition. The focus here is the treatment of problems where there are grounds to reject this hypothesis.

Components vs species

In constructing a phase diagram such as Fig. 1 it is convenient to choose C, O, and H as components; thus fluid composition can be defined in terms of the bulk fractions of the components (Y_i). These fractions are to be distinguished from the concentrations of the molecular species (y_i) that actually comprise the fluid. In particular, the latter vary as a function of pressure and temperature in response to processes of homogeneous fluid phase equilibration, whereas the former are independent of these processes. The partial molar Gibbs energy of any species is expressed as the stoichiometrically weighted sum of the chemical potentials of its components:

$$\bar{G}_i = \sum_{j=1}^c v_j^i \mu_j \quad (2)$$

where v_j^i is the stoichiometric coefficient of component j in species i . The fugacity of the species may then be written:

$$f_i = \exp \left[\frac{\bar{G}_i - G_i^0}{RT} \right] \quad (3)$$

Equations 2 and 3 are not based on any supposition as to the existence of a given species; thus, through these equations it is possible to compute the fugacity of any arbitrarily defined species. Whether or not a species actually exists is thermodynamically irrelevant, but in practice fluid properties are computed as a sum of molecular species properties. Identification of those molecular species present in significant quantity is therefore the key to the accuracy of any computations. In the present context, a species is considered signifi-

cant if its omission would change the chemical potential of any component by more than 100 J/mol. Based on this criterion only H_2 , CH_4 , H_2O , CO and CO_2 were found to be present in significant amounts in GCOH fluids, and O_2 was the only other important species in C–O–H fluids more generally. The atomic fractions of GCOH fluid components are related to the molecular species fractions by the mass balance constraint:

$$Y_j = \frac{\sum_{i=1}^n v_j^i y_i}{\sum_{j=1}^c \sum_{i=1}^n v_j^i y_i} \quad (4)$$

from which it follows that the compositional variable X_O (Eq. 1) can be expressed as:

$$X_O = \frac{Y_O}{Y_O + Y_H} = \frac{y_{H_2O} + y_{CO} + 2y_{CO_2} + 2y_{O_2}}{2y_{H_2} + 4y_{CH_4} + 3y_{H_2O} + y_{CO} + 2y_{CO_2} + 2y_{O_2}} \quad (5)$$

C–O–H fluid speciation as function of X_O

The main concern of this paper is carbon-saturated systems, which under certain circumstances provide a useful model for carbon-undersaturated systems. To understand when these situations are realized GCOH and O–H fluid speciation (Fig. 2a) is reviewed here.

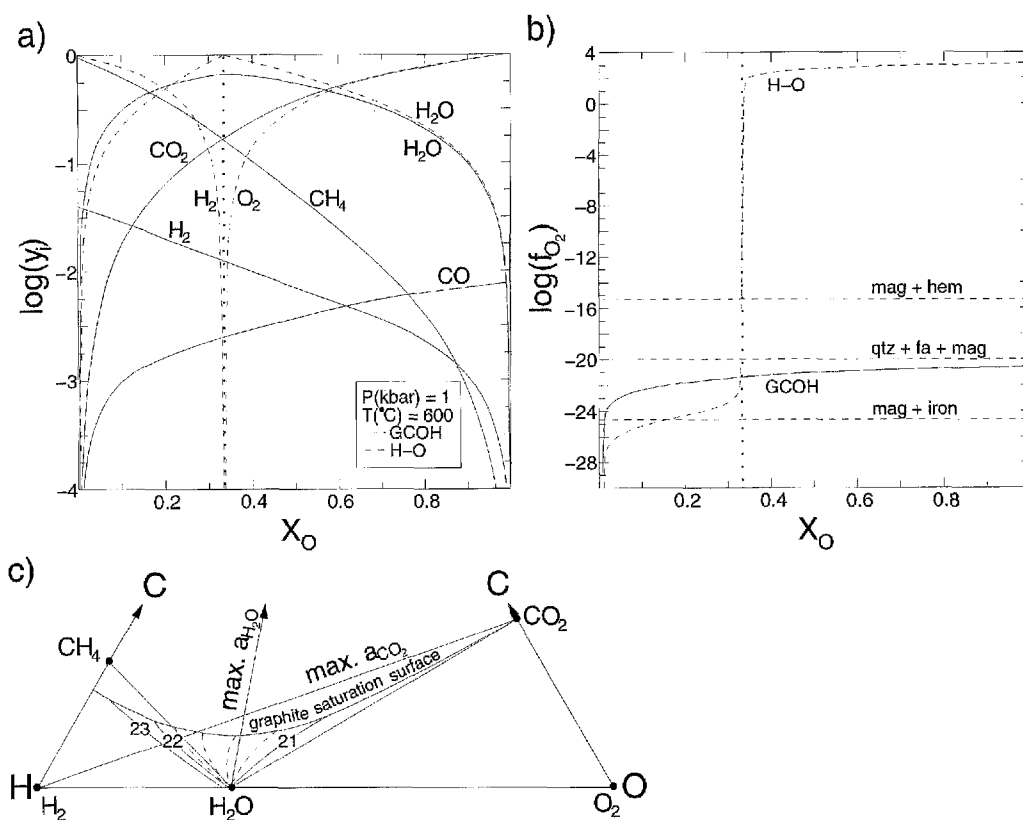
The quantitative position of the carbon-saturation surface (Fig. 2c), and C–O–H molecular species concentrations can be calculated from equations of state as a function of X_O as described in Appendix 1. From mass balance considerations alone, however, $X_O = 0$ and 1 GCOH fluids must consist of CH_4 – H_2 and CO_2 – CO mixtures, respectively. At intermediate X_O values, GCOH fluid consists of finite, although in some cases negligible, amounts of H_2 , CH_4 , H_2O , CO and CO_2 . Even if O_2 is not considered to be a significant species, the f_{O_2} , or more properly μ_{O_2} , of the fluid may be obtained from the partial molar Gibbs energies of other species, c.g., $\mu_{O_2} = \frac{1}{2}(\bar{G}_{CO_2} - G_{\text{graphite}}^0) = \frac{1}{2}(G_{O_2}^0 + RT \ln f_{O_2})$.

An omnipresent feature of C–O–H fluid speciation at P – T conditions characteristic of metamorphic environments is that H_2O is the dominant species at $X_O = \frac{1}{3}$ (Fig. 2a). Except in the vicinity of the $X_O = \frac{1}{3}$ composition, GCOH fluids are nearly binary CH_4 – H_2O and H_2O – CO_2 mixtures; thus taking the binary fluids as limiting models (e.g., $y_{CO_2} = 1 - y_{H_2O}$ for $X_O > \frac{1}{3}$), the fractions of CH_4 and CO_2 are expressed from Eq. 5 as:

$$y_{CH_4} \approx \frac{1 - 3X_O}{X_O + 1}, \quad X_O < \frac{1}{3} \quad (6)$$

$$y_{CO_2} \approx \frac{3X_O - 1}{X_O + 1}, \quad X_O > \frac{1}{3} \quad (7)$$

Fig. 2a–c Calculated O–H (dashed curves) and GCOH (solid curves) fluid speciation (a) and f_{O_2} (b) as a function of X_O at 600°C and 1 kbar. Vertical dotted line marks $X_O = \frac{1}{3}$ composition, horizontal dashed lines in b locate conditions for f_{O_2} buffers. c Variation of $-\log f_{O_2}$ in C–O–H fluid at unit intervals from $-\log f_{O_2} = 23$ to $-\log f_{O_2} = 21$ (solid contours) and at 0.2 log unit intervals about the $X_O = \frac{1}{3}$ composition (dashed contours)



Increasing pressure and decreasing temperature shifts the composition of $X_O = \frac{1}{3}$ GCOH fluid toward the H_2O – CO_2 and H_2O – CH_4 joins (e.g., Ohmoto and Kerrick 1977; Connolly and Cesare 1993), improving the accuracy of these approximations. Similar relationships can be written, that hold with greater rigor, for the speciation of O–H fluid on either side of the $X_O = \frac{1}{3}$ composition.

The species abundances shown in Fig. 2a reflect the fundamental thermodynamic constraint that the activity of a species must be a maximum when the fluid and the species have the same composition (Appendix 2). This constraint implies that in a compositional section taken such that the chemical potential of one component remains constant (as on the carbon-saturation surface), the activity of a species must reach a maximum when the proportions of the unconstrained components in the fluid and species are identical. Thus C–O–H fluid compositions at which a_{H_2O} and a_{CO_2} are maximized correspond to the H_2O –C and CO_2 – H_2 joins, respectively (Fig. 2c). Coincidence of maxima in activity and concentration for a multicomponent species is not thermodynamically required in a nonideal fluid, as it is for a one-component species, but can often be assumed as a good approximation, particularly for H_2O . Therefore, the common statement

that metamorphic dehydration reactions buffer fluid composition toward the maximum water-content possible for the fluid is not strictly correct, but it is valid for most practical purposes (Connolly and Cesare 1993).

Although thermodynamic constraints require that the f_{O_2} of C–O–H fluids increase with X_O along both the O–H join and the carbon-saturation surface, the X_O – f_{O_2} relationships in these systems are very different (Fig. 2b). In the O–H system, $X_O = \frac{1}{3}$ fluid is effectively pure water, and f_{O_2} is poorly defined between the highly reduced and oxidized values characteristic of the H_2 – H_2O and H_2O – O_2 binaries. Indeed the variation in f_{O_2} across the $X_O = \frac{1}{3}$ composition of O–H fluids, which is accentuated with decreasing temperature or increasing pressure, easily encompasses the range of f_{O_2} characteristic of crustal environments. Thus where an O–H fluid model is appropriate, variation in X_O is unlikely to be significant; this is borne out by phase equilibria in highly reduced alloy-bearing serpentinites that indicate $X_O = 0.332$ – 0.3332 (Peretti and Connolly in prep). In contrast to O–H fluid, abundances of secondary species in GCOH fluid are sufficient to ensure smooth variation in f_{O_2} over the entire range of X_O . Inasmuch as H_2O is the dominant constituent of geologic fluids, the $X_O = \frac{1}{3}$ composition can be taken as

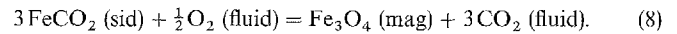
a neutral point for characterizing the redox state of mineral-fluid equilibria. GCOH fluids are unlikely to be generated¹ on the reduced side of the $X_O = \frac{1}{3}$ composition because mineral devolatilization liberates water, CO_2 and O_2 . The minor variation of f_{O_2} in GCOH fluid at $X_O > \frac{1}{3}$ accounts for the monotony of opaque mineralogy in graphitic rocks (Whalen and Chappell 1988; Frost 1990). Ideally the $X_O = \frac{1}{3}$ composition should coincide with conditions of constant f_{O_2} in the C–O–H composition space; as seen in Fig. 2c, this situation is nearly realized. In detail, at $X_O = \frac{1}{3}$, O–H fluid is considerably more oxidized than GCOH fluid, with the result that there is an abrupt increase in the f_{O_2} of $X_O = \frac{1}{3}$ C–O–H fluid at very low Y_C (Fig. 3b), although the variation is otherwise negligible.

Because the O–H join represents both the reduced and oxidized extremes of C–O–H fluids, GCOH fluids are the most oxidized and reduced fluids possible at $X_O > \frac{1}{3}$ and $X_O < \frac{1}{3}$, respectively (Figs. 2b, 2c, 3b). This implies that the process of graphite precipitation is one of oxidation in $X_O < \frac{1}{3}$ fluids (Frost 1979a), and that the maximum f_{CO_2} of $X_O < \frac{1}{3}$ fluids occurs at the carbon-saturation surface. At $X_O > \frac{1}{3}$ species other than H_2O , CO_2 , and CO become negligible in GCOH fluids. The composition of fluids composed dominantly of those species must lie in the triangular region of C–O–H composition space bounds by the H_2O , CO_2 , and CO (Fig. 1). Thus as fluid composition shifts away from the carbon-saturation surface toward the H_2O – CO_2 join, the abundance of O_2 must increase such that $y_{\text{CO}_2} X_{\text{CO}_2} = 2 y_{\text{O}_2}$ at the H_2O – CO_2 join² (Fig. 3a). The increase in y_{O_2} leads to anomalously high values of f_{O_2} at the H_2O – CO_2 join (Fig. 3b); natural $X_O > \frac{1}{3}$ C–O–H fluids must therefore be restricted to the narrow field between the carbon-saturation surface and the H_2O – CO_2 join. When the CH_4 – H_2O join lies within the fluid composition space it plays a similar role in that it defines a transition from reduced to very reduced fluids (Fig. 3b). This transition is less pronounced because H_2 is a significant, though minor, species along the carbon-saturation surface at $X_O < \frac{1}{3}$ (Fig. 3a).

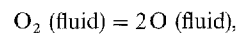
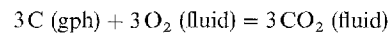
Principles of P – T – X_O phase diagram projection

As isobaric-isothermal GCOH fluid speciation is defined solely as a function of X_O it can be anticipated that methods of interpretation and calculation P – T – X_O diagrams are similar to those employed for

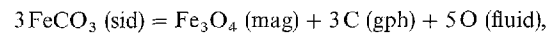
systems with a binary fluid. There is, however, an important distinction in that X_O relates the properties of three chemical components and this introduces complexities. Consider the siderite-magnetite equilibrium:



Prediction of the geometry of this equilibrium in P – T – X_O space is not obvious because both f_{O_2} and f_{CO_2} increase with X_O . This difficulty arises because although GCOH fluids are characterized by a single compositional parameter, and are therefore truly two-component solutions in a thermodynamic sense (Connolly 1990), oxide equilibria are conventionally written in terms of species, which may not be independently variable. From equilibrium Eq. 8 this becomes apparent from the equilibria:



which can be combined with Eq. 8 to obtain:



from which it is evident that increasing X_O , which must increase μ_{O} , but cannot affect μ_{C} , favors reduction of magnetite to produce siderite. Any equilibrium written with complex C–O–H fluid species can be rewritten by such manipulations in terms of the one-component species H and O, and graphite. As μ_{C} is independent of X_O , and μ_{H} and μ_{O} are monotonic functions of X_O , P – T – X_O phase diagram projections are analogous to the well known P – T – X_{CO_2} diagrams.

The analogy between P – T – X_O and P – T – X_{CO_2} diagrams is made more elegantly by noting that if a system is in equilibrium with graphite at all conditions of interest, then the phase relations of the system can be described with no loss of information in a carbon-free subcomposition. In petrologic jargon, this reduction in the dimensionality of the composition space is said to be accomplished by “projection” through carbon. The thermodynamic equivalent of this projection is the Legendre transformation of the Gibbs energy for the system and its constituent phases:

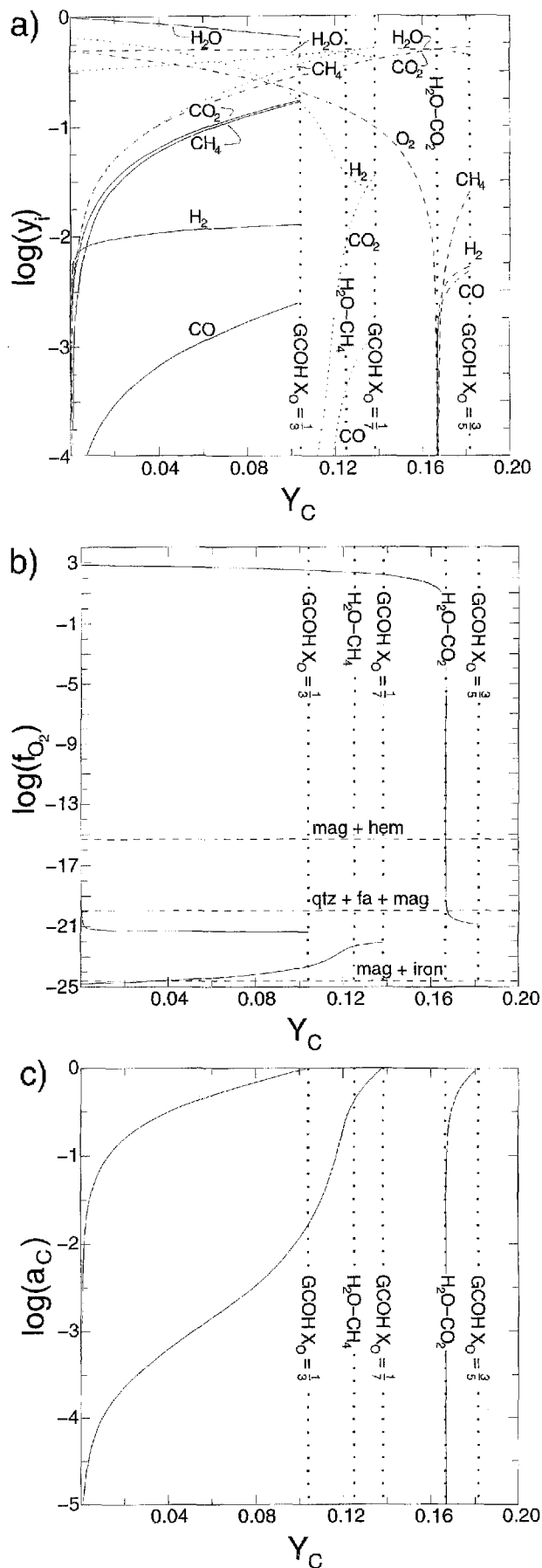
$$\Omega = G - n_{\text{C}}\mu_{\text{C}}, \quad (15)$$

where $\mu_{\text{C}} = G_{\text{graphite}}^{\circ}$ and the free energy function Ω is minimized for an isobaric-isothermal equilibrium.

There are no simple geologic systems that simultaneously involve redox, dehydration, and decarbonation equilibria, so for purposes of demonstration consider a hypothetical four component system M–C–O–H in which up to six phases may be stable: fluid, graphite, and four compounds A ($\text{M}(\text{OH})_2$), B ($\text{M}(\text{OH})_3$), C (M_2O_3), and D (MCO_3 , or, in the carbon-free subcomposition, MO_3). In the GCOH fluid-saturated portion of this system, at specified pressure or temperature,

¹ The term generated is used here to imply the generation of fluid from a fluid-absent initial condition, this excludes processes by which pre-existing fluids are modified through fluid-rock interaction.

² For the composition of C–O fluid to be that of CO_2 , y_{CO} must be $2y_{\text{O}_2}$. To the extent that the abundances of CH_4 and H_2 are negligible, it follows that the minimum y_{O_2} must be linearly proportional to X_{CO_2} as composition shifts away from the C–O join.



the possible univariant equilibria are the six permutations of the four compounds taken two at a time. These permutations, labeled by the identities of the compounds not present in the equilibrium, are listed in Table 2. The associated reaction equations can be written in any number of ways in terms of C-O-H volatile species, as done in the second column of Table 2 using the species H_2O , CO_2 , and O_2 . Alternatively, if reactions are written with the fluid components H and O, after projection through carbon, there are only two types of reactions possible (Table 2, third column): Type I reactions in which the reaction coefficients (v_H , v_O) of the volatile components have the same sign, or one coefficient is zero, ((A, B) (B, C), (B, D), (A, C), (C, D)); and Type II reactions in which the reaction coefficients of the volatile components have opposite signs ((A, D)).

It can be demonstrated by analogy with the arithmetic arguments put forward for the construction of $T-X_{CO_2}$ and $P-X_{CO_2}$ diagrams (e.g., Greenwood 1962)³, that the $T-X_O$ or $P-X_O$ phase field corresponding to a type I reaction must have an extremum at $X_O = v_O / (v_O + v_H)$, whereas the loci of the equilibrium of a type II reaction must approach the limiting fluid compositions asymptotically with no intervening extremum. The chemographic distinction between type I and II reactions is seen in Fig. 4 to be that the compositions of the condensed phases of a type I reaction must lie along a line, or a plane in more complex systems, that intersects a possible composition of the fluid (e.g., the reactions corresponding to ((A, B), (A, C), (B, C), (B, D), (C, D)). It follows that if a system is initially composed of only the fluid-absent assemblage of a type I reaction, then this assemblage may devolatilize to produce a fluid, and that this fluid can have only one composition, i.e., $X_O = v_O / (v_H + v_O)$. Such reactions are also known as *singular reactions*, because they are a degenerate form of more general fluid-producing reactions. The composition of the fluid produced by a singular reaction is a *singular composition*. The geometry of

Fig. 3a-c Calculated C-O-H fluid speciation (a), f_{O_2} (b), and a_C (c) as a function of Y_C at $X_0 = \frac{1}{3}$ (solid curves) $X_0 = \frac{2}{3}$ (short dashed curves), and $X_0 = \frac{1}{2}$ (long dashed curves) at 600°C and 1 kbar. The latter two compositions are those at which GCOH fluid has $X_{CH_4} \approx \frac{1}{2}$ and $X_{CO_2} \approx \frac{1}{2}$, respectively, from Eqs. 6 and 7. Vertical dotted lines locate positions of carbon-saturation surface, H_2O-CO_2 join at $X_0 = \frac{2}{3}$, and CH_4-H_2O join at $X_0 = \frac{1}{2}$. Horizontal dashed lines in b locate conditions for f_{O_2} buffer assemblages

³ Greenwood's arithmetic arguments regarding extrema of type I equilibria can be made more simply and generally by noting that if it were possible to have an extremum at any composition other than $X_O = v_O / (v_H + v_O)$, then equilibrium would not be possible at fluid compositions between the extremum and the composition $X_O = v_O / (v_H + v_O)$ because reaction progress would drive fluid composition away from the equilibrium composition. A third, alternative, argument on the location of $P-T-X_O$ extrema is given in Appendix 2.

Table 2 Possible $T-X_O$ univariant equilibria and reactions in the GCOH fluid-saturated system M-C-O-H. Reaction coefficients of products and reactants are considered to have opposite signs. Equilibria are identified by the phases possible in the system, but absent from the equilibrium. Phase chemography is shown in Fig. 4, phase notation: A ($M(OH)_3$), B (MCO_3 or MO_3), C ($M(OH)_2$), and D (M_2O_3)

Equilibrium	Reaction	Projected Reaction	Extremum Point
(C, D)	$M(OH)_3 + \frac{3}{4}O_2 = MCO_3 + \frac{3}{2}H_2O$	$M(OH)_3 = MO_3 + 3H$	$f_1, X_O = 0$
(A, B)	$2M(OH)_2 + \frac{1}{2}O_2 = M_2O_3 + 2H_2O$	$2M(OH)_2 = M_2O_3 + 4H + O$	$f_2, X_O = \frac{1}{3}$
(B, C)	$2M(OH)_3 = M_2O_3 + 3H_2O$	$2M(OH)_3 = M_2O_3 + 6H + 3O$	$f_3, X_O = \frac{1}{3}$
(B, D)	$M(OH)_3 = M(OH)_2 + \frac{1}{2}H_2O + \frac{1}{4}O_2$	$M(OH)_3 = M(OH)_2 + H + \frac{3}{2}O$	$f_4, X_O = \frac{3}{5}$
(A, C)	$2MCO_3 + \frac{1}{2}O_2 = M_2O_3 + 2CO_2$	$2MO_3 = M_2O_3 + 3O$	$f_5, X_O = 1$
(A, D)	$M(OH)_2 + CO_2 = MCO_3 + H_2O$	$M(OH)_2 + O = MO_3 + 2H$	None

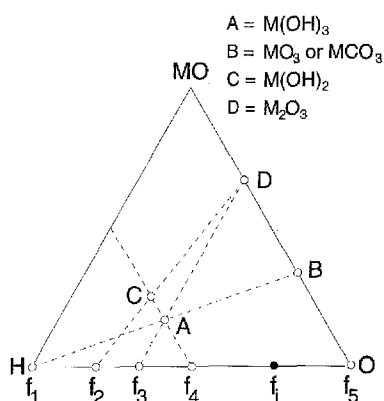


Fig. 4 Chemographic relations in the hypothetical M-C-O-H system in the M-O-H subcomposition after projection through carbon. The fluid composition intersected by the *dashed line* connecting any pair of compounds is that produced by decomposition of the more volatile-rich compound, i.e., the X_O coordinate of the extremum points in Fig. 5 (see also Table 2). Composition f_i is the fluid composition at the invariant point in Fig. 6

phase fields of type I reactions is constrained further given that the fluid-present assemblage of the reaction tends to have greater entropy and volume than its fluid-absent equivalent. Thus, the fluid-present assemblage is generally stable on the high-temperature and low-pressure side of type I phase fields, although exceptions to the latter generality are not uncommon. In contrast to type I reactions, the compositions of the condensed phases of type II reactions define a line, or plane, that does not span any possible fluid composition (e.g., (A, D), Table 2 and Fig. 4). Consequently, type II reactions can only occur in the presence of a fluid, but they cannot generate a fluid.

Given the constraints discussed in the foregoing paragraph, the isobaric $T - X_O$ diagram for the hypothetical graphite- and fluid-saturated M-C-O-H system shown in Fig. 5 was constructed by assuming stability of invariant fields [A] and [D]. The utility of such a diagram is that it indicates the likely influence of

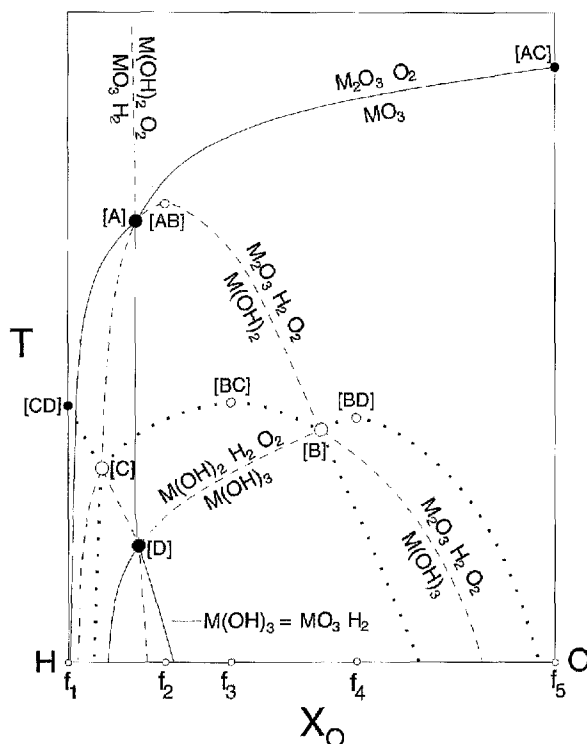


Fig. 5 Isobaric $T-X_O$ phase diagram section for the carbon-saturated M-C-O-H system. Invariant and singular points are identified by the phases possible in the system, but absent from the equilibrium, in *square brackets*. Stable, singly metastable, and doubly metastable univariant fields are shown by *solid*, *dashed*, and *dotted curves*, respectively

devolatilization equilibria on the fluid evolution of graphitic rocks. A simple dehydration equilibrium such as (B, C) must have a $T - X_O$ maximum $X_O = \frac{1}{3}$; thus such reactions must buffer fluid composition toward this composition during prograde metamorphism (cf. Ohmoto and Kerrick 1977; Connolly and Cesare 1993); whereas decarbonation or deoxygenation equilibria such as (A, C) buffers fluid composition toward $X_O = 1$. Simple mineral devolatilization reactions cannot

coefficient of one phase in the reaction of the non-degenerate field changes sign, e.g., across the [B, D] singular point the reaction equation of (D) changes from $A = B + C + F$ to $A + B = C + F$ with decreasing pressure.

An asset of the P - T projection is that it defines the stability of the relevant phases not only for all possible fluid compositions, but also for fluid-absent conditions. As an example of this the inset of Fig. 6 shows the stability field of the assemblage $B + C$ to be bound by univariant fields (F) and (A), and that of $B + C + F$ to be bound by (D) and (A). Considering the M-C-O-H chemographic relations (Fig. 4), it can be deduced that on either side of (D) there are two possible assemblages that include $B + C$. These are $A + B + C$ or $B + C + D$, and $B + C + D$ or $B + C + F$ at low and high temperature, respectively.

The construction of the P - T projection shown in Fig. 6 brings to light two errors in earlier discussions of projections for mixed-volatile fluids that merit mention. Abart et al. (1992) stated that any singular equilibrium for which fluid composition is extremal, i.e., $X_O = 0$ or 1, cannot become metastable in a $(c + 2)$ -phase system. This statement supposes that the compositions of the phases of the singular equilibrium lie at a boundary of the possible composition space for the system; however, as demonstrated by equilibrium (C, D), it is possible that the phase compositions in such an equilibrium span the composition space of the system. In this case the equilibrium can have any permitted level of stability. Connolly and Trommsdorff (1991) showed a topology where non-degenerate univariant fields terminate at singular points at which fluid composition is extremal. Although this is a valid topological device, and does not violate any fundamental thermodynamic principle, it implies a phenomenological extreme that is unlikely to be realized; specifically here, the possibility that a hydrogen-bearing compound coexists with a hydrogen-free fluid. Thus in real phase diagram projections such singular points do not occur, and the conjugate univariant fields must approach the relevant singular field asymptotically, e.g., as (A) and (C) approach (A, C), and (C) and (D) approach (C, D).

Fluid-absent T - X_O invariant reactions

As a result of compositional degeneracies it is not uncommon that the equilibrium of a "fluid-absent" reaction, i.e., a reaction in which the reaction coefficient of the fluid is zero, appears in T - X_O projection. It is important to recognize such an equilibrium, in particular if it projects as a T - X_O invariant point, to avoid making incorrect inferences as to possible fluid compositions that can be generated by mineral devolatilization. To illustrate this, consider the carbon-saturated, M-C-O-H system comprised of fluid, and

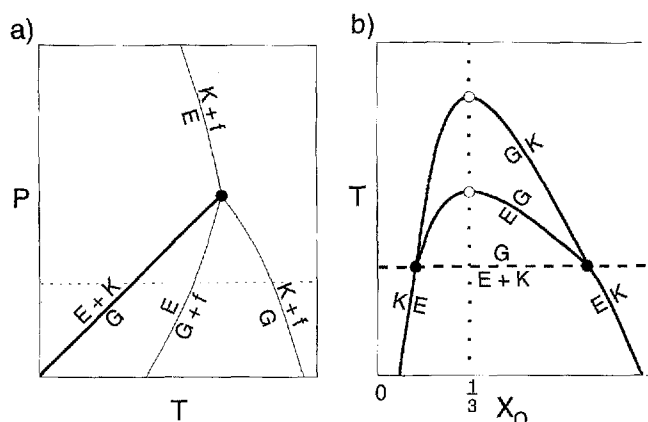


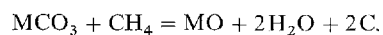
Fig. 7a, b Phase relations for a carbon-saturated M-C-O-H system in which the only compounds other than graphite are E ($M(OH)_2$), G ($M_2O(OH)_2$) and K (MO). a P - T projection, the univariant dehydration equilibria correspond to singular reactions that generate an $X_O = \frac{1}{3}$ fluid (f), dotted line locates isobaric T - X_O section (b). In b, $G = E + K$ is stable at the T - X_O invariant points, but metastable at all other fluid compositions

the compounds E ($M(OH)_2$), G ($M_2O(OH)_2$), and K (MO). As the compounds differ only in degree of hydration, the only possible univariant devolatilization reactions correspond to the $X_O = \frac{1}{3}$ singular equilibria $E = G$, $E = K$, and $G = K$. Given the orientation of the univariant fluid-absent phase field $G = E + K$ shown in the P - T projection of Fig. 7a, the topology of the singular curves can be determined by Schreinemakers principles. If an isobaric T - X_O section is constructed at any pressure below that of the invariant point of the P - T projection, the univariant T - X_O phase fields $G = K$ and $E = G$ must intersect at two invariant points representing the fluid-absent equilibrium $G = E + K$. In this context fluid-absent is perhaps a misnomer, in that although the reaction does not involve fluid, it is stable in the presence of a fluid with compositions corresponding to the X_O coordinates of the invariant points. Thus, the impression that devolatilization of the assemblage $E + K$ at the T - X_O invariant points is capable of generating highly reduced or oxidized fluids is false. The system would be capable of attaining such conditions only by buffering the composition of an even more reduced or oxidized, externally derived, fluid through dehydration. In the absence of an externally derived fluid, dehydration would only occur at the $X_O = \frac{1}{3}$ composition.

Graphite reaction coefficients

The reaction coefficient of graphite in the reaction associated with a univariant P - T phase field can only be determined if the carbon-content of the fluid is known at the conditions of interest. As the carbon-saturation surface lies at more carbon-rich compositions

than the $\text{H}_2\text{O}-\text{CO}_2$ join (Fig. 2c), it is possible to make the generalization that any fluid-generating reaction that does not involve both decarbonation and a redox process must consume graphite. In contrast to reactions that involve redox processes, the reaction coefficient of graphite tends to be small in dehydration-decarbonation reactions because of the proximity of the carbon-saturation surface to the $\text{H}_2\text{O}-\text{CO}_2$ join. Univariant P - T fields correspond to the invariant and singular points of isobaric T - X_{O} diagrams; therefore a definite stoichiometry can be assigned to the reactions that occur at the conditions represented by these points. However, the reaction coefficient of graphite for reactions that occur along the univariant T - X_{O} phase fields between invariant and singular points may vary strongly as a function of X_{O} , and cannot be quantitatively constrained without knowledge of the proportions of fluid and mineral reactants. Consider decarbonation of MCO_3 to MO . At $X_{\text{O}} = 1$ this reaction must consume graphite because GCOH fluid is slightly more carbon-rich than CO_2 , but at $X_{\text{O}} < \frac{1}{3}$ the dominant fluid species are CH_4 and H_2O and the reaction stoichiometry must approach:



Even if the decarbonation equilibrium occurs only at $X_{\text{O}} > \frac{1}{3}$, as commonly the case, irregular variation of the carbon-saturation surface relative to the $\text{H}_2\text{O}-\text{CO}_2$ join, discussed subsequently with regard to metasomatic processes, may lead to a situation in which graphite is precipitated with increasing X_{O} . For these reasons, it is misleading to assign graphite reaction coefficients for P - T - X_{O} phase fields.

A petrogenetic grid for the graphitic system $\text{C-O-H-FeO-TiO}_2\text{-SiO}_2$

The system $\text{C-O-H-FeO-TiO}_2\text{-SiO}_2$ is employed here to demonstrate the methods discussed previously. Calculations for this system were done taking into consideration the phases fayalite, ferrosilite, grunerite, ilmenite, magnetite, quartz, rutile, siderite, and GCOH fluid (see Table 1 for notation). Ilmenite and magnetite were treated as Fe-Ti solutions with mixing properties as described by Anderson and Lindsley (1988). Thermodynamic data for all minerals were taken from a revised version of Holland and Powell's (1990) data base. Properties of the fluid were computed as in Connolly and Cesare (1993). The calculations were done using a computer program (Connolly 1990) that is available from the author. For calculations in which the composition of phases are implicit variables, the program computes equilibrium compositions with a specified precision. In the present case, the compositional precision for

magnetite, ilmenite, and fluid were set to ± 4 , ± 0.5 , and ± 0.1 mol%, respectively. Where cited, estimated standard errors (\hat{s}) on equilibrium conditions were computed from the variance-covariance matrix for the thermodynamic data as estimated from Holland and Powell's (1990) regression analysis of experimental data. Aspects of the $\text{C-O-H-FeO-TiO}_2\text{-SiO}_2$ system were considered by Connolly and Cesare (1993) using an earlier version of Holland and Powell's data; the calculated equilibria presented here are substantially different and should be considered to supersede those presented earlier. In particular, the stability field of Fe-amphibole is reduced, in agreement with the recent experiments of Lattard and Evans (1992), and the stability of magnetite expanded, in better agreement with natural assemblages, as discussed below. For simplicity, equilibria involving native iron and wüstite, that are stable at $X_{\text{O}} < 0.05$, are not considered because such conditions are unlikely to be realized in crustal metamorphic environments where the $\text{C-O-H-FeO-TiO}_2\text{-SiO}_2$ system is an appropriate model.

Calculated isobaric T - X_{O} sections and the P - T projection for the graphite-saturated $\text{C-O-H-FeO-TiO}_2\text{-SiO}_2$ system are shown in Figs. 8 and 9, respectively. To clarify these diagrams, Fig. 10 shows the fluid- and graphite-saturated phase relations at various conditions represented in Fig. 8, and the compositions of coexisting phases at selected points in Figs. 8 and 9 are listed in Table 3. In Fig. 8, phase fields in the C-O-H-FeO-SiO_2 and $\text{C-O-H-FeO-TiO}_2\text{-SiO}_2$ systems are distinguished by thin and thick lines. For example, in Fig. 8a, the phase field $\text{sid} = \text{mag}$ corresponds to conditions for the equilibrium of the reaction (with graphite and fluid) that defines the absolute stability of siderite, and the lower thermal limit for stoichiometric magnetite in the presence of graphite and C-O-H -fluid; whereas, the phase field $\text{sid} + \text{Ilm} = \text{Mag}$ defines the lower thermal limit of magnetite-ulvöspinel solution coexisting with graphite and fluid. The limiting composition of the magnetite-ulvöspinel solution, at the conditions represented by Fig. 8a, can be determined, from Table 3, to vary from Mag_{98} at its reduced, low-temperature, extreme (point P_2) to Mag_{86} at the singular point P_6 .

In contrast to most other carbonate-bearing systems, the $\text{C-O-H-FeO-TiO}_2\text{-SiO}_2$ system is relatively simple in that the only stable singular equilibria involving fluid occur at $X_{\text{O}} = \frac{1}{3}$ or 1 at conditions shown in Fig. 9. The $X_{\text{O}} = \frac{1}{3}$ (F_{33}) singular curves (Fig. 9a) define the maximum stability for grunerite in the presence of graphite. These curves locate the conditions for grunerite dehydration in the absence of siderite or magnetite, and essentially reproduce the $\text{H}_2\text{O-FeO-SiO}_2$ petrogenetic grid of Lattard and Evans (1992), demonstrating the negligible effect of graphite in simple dehydration processes (Connolly and Cesare 1993).

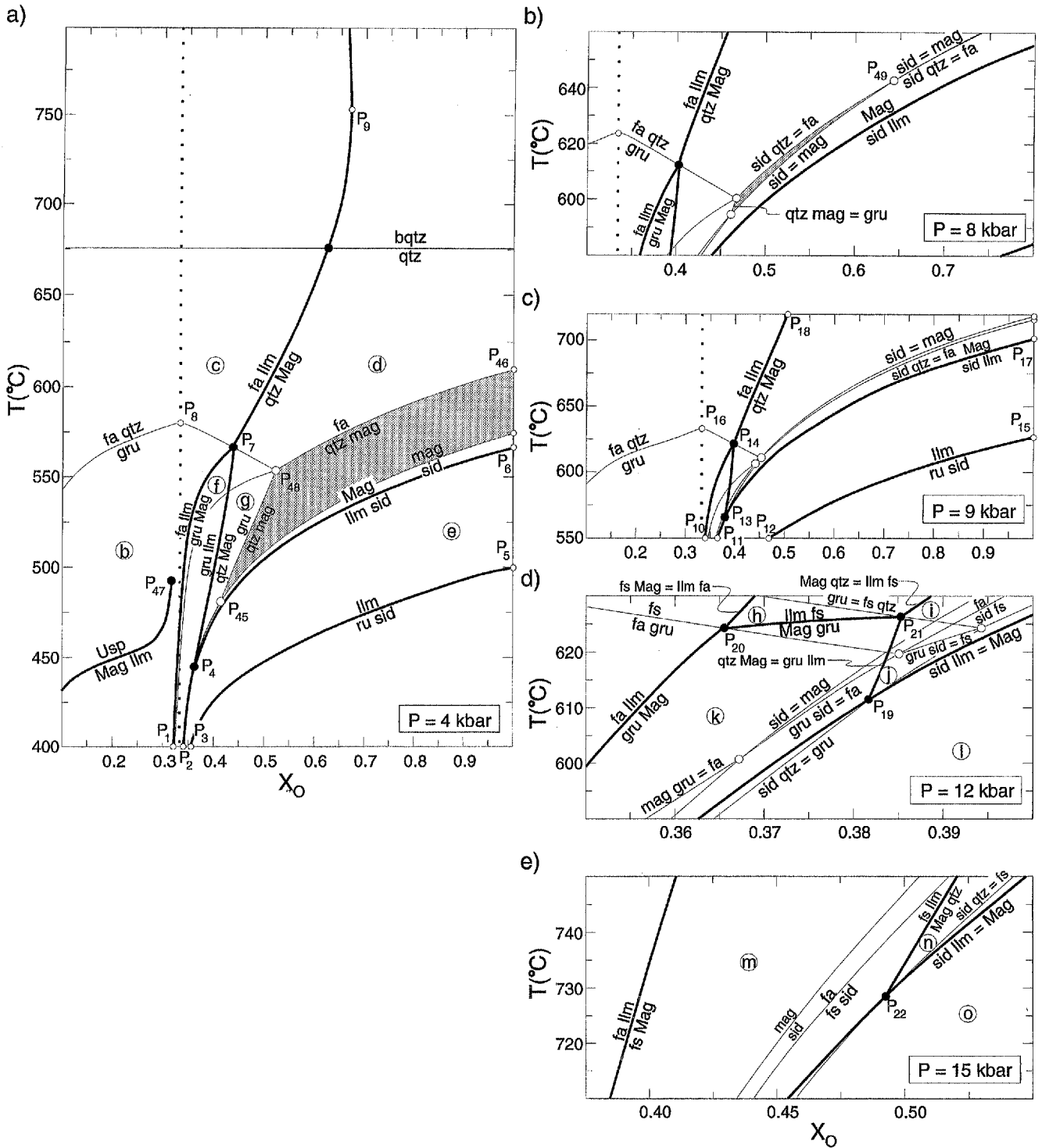


Fig. 8a-e Calculated isobaric T - X_0 phase diagram sections for the carbon-saturated C-O-H-FeO-TiO₂-SiO₂ system. Thin curves represent C-O-H-FeO-SiO₂ equilibria; mag + qtz field (stable in **a** and **b**) is shaded. Where reactions are written on a single line, the high T assemblage is to the right. Large open and filled circles represent C-O-H-FeO-SiO₂ and C-O-H-FeO-TiO₂-SiO₂ invariant points, small circles in the interior of the diagrams and on

vertical axes locate extremum points. Circled letters locate conditions for chemographies of Fig. 10. Phase assemblages and compositions at labeled points are listed in Table 3. The univariant field Mag + Ilm = Usp terminates at the critical point P₄₇, at temperatures above this point there is continuous, although not complete, solution between usp and mag. Vertical dotted line locates $X_0 = \frac{1}{3}$ composition

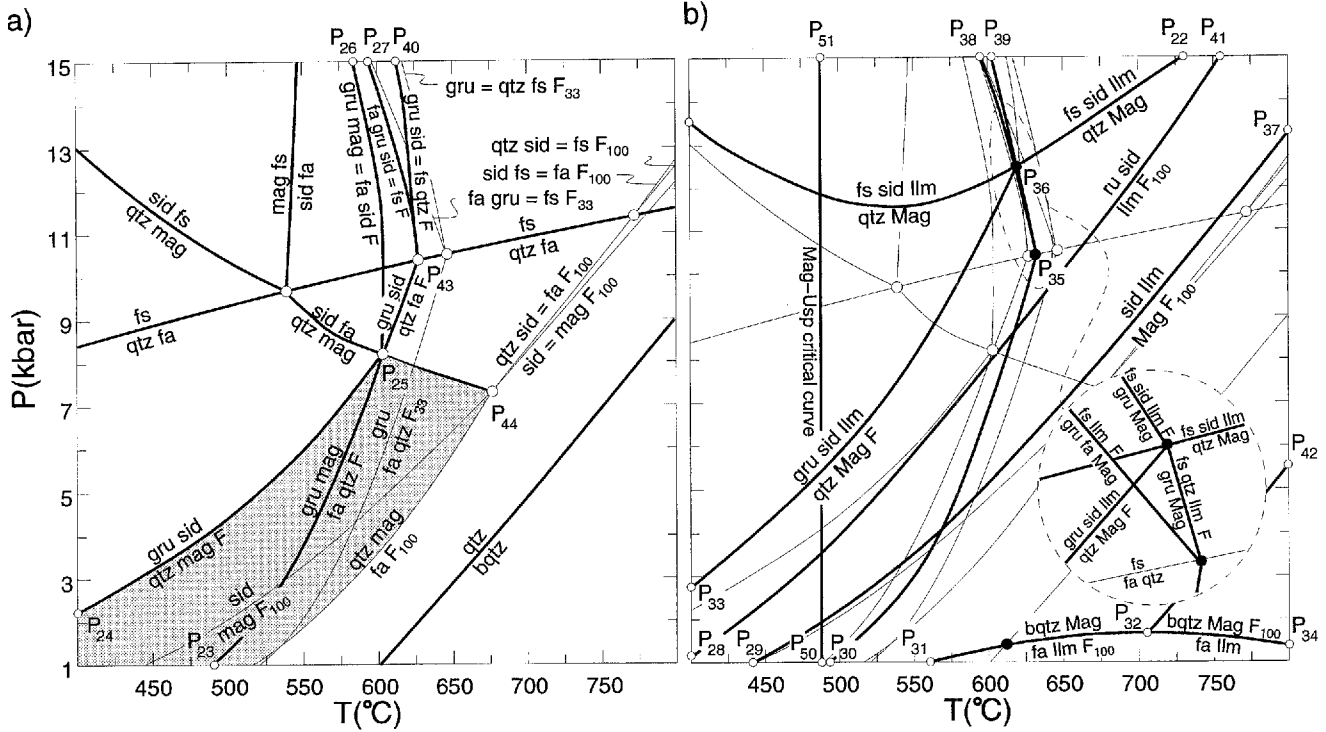


Fig. 9a, b Calculated P - T projection for the graphite-saturated C - O - H - FeO - TiO_2 - SiO_2 system. **a** Equilibria in C - O - H - FeO - SiO_2 subsystem, thin curves represent singular curves, mag + qtz field is shaded. **b** C - O - H - FeO - TiO_2 - SiO_2 univariant fields, thin curves

locate C - O - H - FeO - SiO_2 equilibria of **a**. Phase assemblages and compositions at labeled points are listed in Table 3. T - X_O diagrams of Fig. 8 are isobaric fluid-saturated sections of portions of the P - T projection

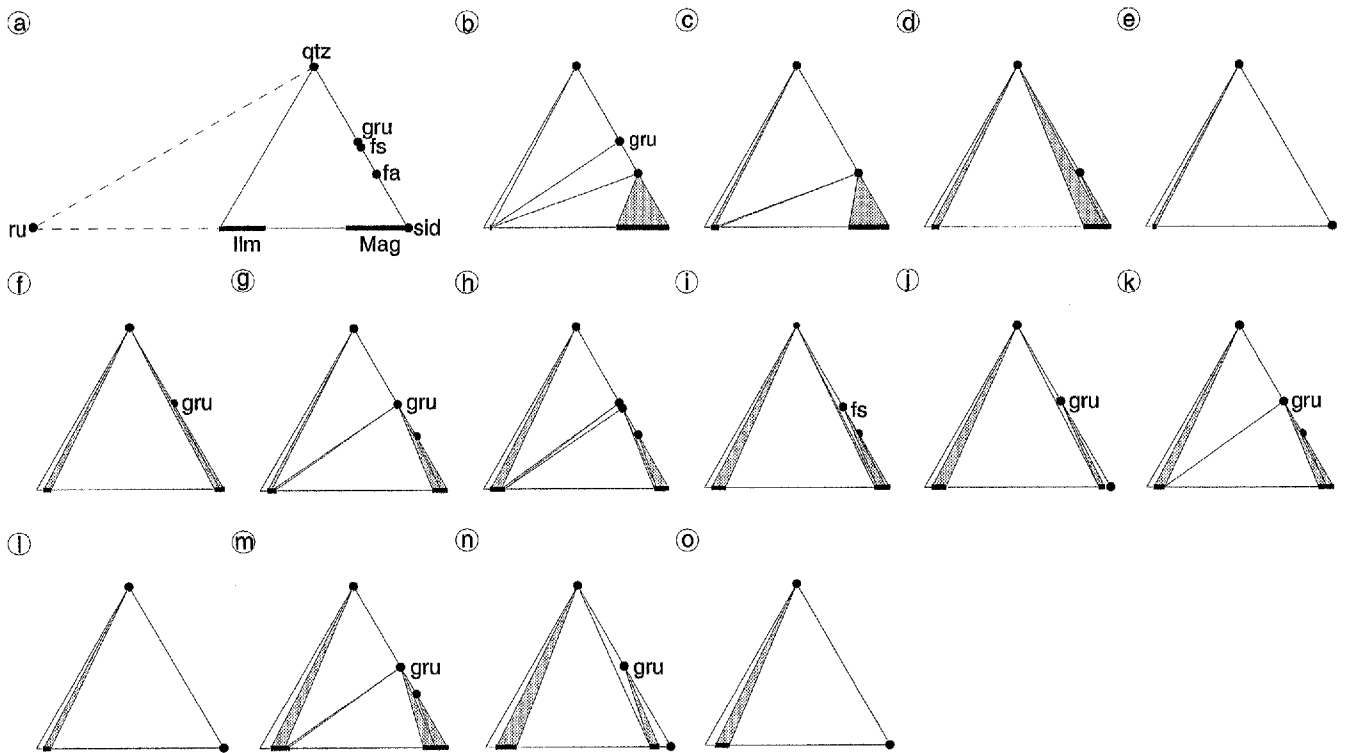


Fig. 10a-o Calculated chemographic relations for the fluid- and graphite-saturated C - O - H - FeO - TiO_2 - SiO_2 system at conditions indicated in Fig. 8. Compounds are identified by filled circles and the composition of solutions are indicated by heavy solid bars as in **a**;

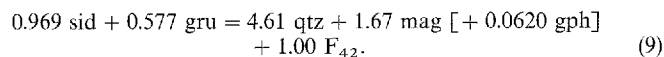
shaded regions are two-phase fields. In **b-o** only the composition space bound by compositions $FeTiO_3$ - SiO_2 - FeO is shown (the triangle drawn with solid lines in **a**). At all conditions illustrated, the most ilmenite-rich Ilm coexists with qtz + ru

Table 3 Phase assemblages corresponding to points in Fig. 8 and 9, notation as in Table 1; fluid is not listed for assemblages identified only in Fig. 8. The additional phase that coexists with degenerate assemblages is indicated in square brackets

Point	Assemblage	Point	Assemblage
P ₁	fa + gr _u + Ilm ₉₈ + Mag ₉₄	P ₂	[gr _u +]sid + Ilm ₉₈ + Mag ₉₈
P ₃	[qtz +]ru + sid + Ilm ₉₉	P ₄	gr _u + qtz + sid + Ilm ₉₇ + Mag ₉₄
P ₅	[qtz +]ru + sid + Ilm _{98.5}	P ₆	[qtz +]sid + Ilm ₉₆ + Mag ₈₂
P ₇	fa + gr _u + qtz + Ilm ₉₆ + Mag ₇₀	P ₈	fa + gr _u + qtz[+ Ilm ₉₈]
P ₉	fa + qtz + Ilm ₉₅ + Mag _{35.5}	P ₁₀	fa + gr _u + Ilm ₉₈ + Mag ₉₄
P ₁₁	gr _u + sid + Ilm ₉₈ + Mag ₉₈	P ₁₂	[qtz +]ru + sid + Ilm ₉₉
P ₁₃	gr _u + qtz + sid + Ilm ₉₅ + Mag ₈₆	P ₁₄	fa + gr _u + qtz + Ilm ₉₅ + Mag ₇₀
P ₁₅	[qtz +]ru + sid + Ilm _{97.5}	P ₁₆	fa + gr _u + qtz + Ilm _{96.5}
P ₁₇	[qtz +]sid + Ilm ₉₃ + Mag ₆₆	P ₁₈	fa + qtz + Ilm ₉₃ + Mag ₄₅
P ₁₉	gr _u + qtz + sid + Ilm ₉₄ + Mag ₈₂	P ₂₀	gr _u + fa + fs + Ilm ₉₄ + Mag ₇₈
P ₂₁	fs + gr _u + qtz + Ilm ₉₄ + Mag ₇₈	P ₂₂	fs + sid + qtz + Ilm ₉₁ + Mag ₇₀ + F ₄₉
P ₂₃	fa + gr _u + qtz + mag + F ₆₂	P ₂₄	gr _u + qtz + sid + mag + F ₃₆
P ₂₅	fa + gr _u + qtz + sid[+ mag] + F ₄₃	P ₂₆	fa + gr _u + sid + mag + F ₃₄
P ₂₇	fa + fs + gr + sid[+ Mag ₉₈] + F ₃₅	P ₂₈	[qtz +]ru + sid + Ilm ₉₈ + F ₁₀₀
P ₂₉	[fa +]qtz + Ilm ₉₇ + Mag ₄₉ + F ₁₀₀	P ₃₀	fa + gr _u + qtz + Ilm ₉₇ + Mag ₈₂ + F ₃₅
P ₃₁	fa + qtz + Ilm ₉₇ + Mag ₄₉ + F ₁₀₀	P ₃₂	fa + bqtz + Ilm ₉₆ + Mag _{32.5} + F ₁₀₀
P ₃₃	gr _u + qtz + sid + Ilm ₉₈ + Mag ₉₄ + F ₃₅	P ₃₄	fa + bqtz + Ilm ₉₇ + Mag ₂₆ + F ₁₀₀
P ₃₅	fa + fs + gr _u + qtz + Ilm ₉₄ + Mag ₇₄ + F ₃₉	P ₃₆	fs + gr _u + sid + qtz + Ilm ₉₄ + Mag ₇₈ + F ₃₈
P ₃₈	fa + fs + gr _u + Ilm ₉₅ + Mag ₈₂ + F ₃₄	P ₃₉	fs + gr _u + sid + Ilm ₉₄ + Mag ₈₆ + F ₃₅
P ₄₀	fs + gr _u + qtz + sid[+ Ilm ₉₄] + F ₃₆	P ₄₁	[qtz +]ru + sid + Ilm ₉₆ + F ₁₀₀
P ₄₂	fa + qtz + Ilm ₉₅ + Mag _{35.5} [+ F ₆₃]	P ₄₃	fa + gr _u + qtz + sid[+ Mag ₉₄] + F ₄₂
P ₅₀	[fa +]Ilm ₉₈ + Mag ₃₁ + F ₃₄	P ₅₀	[fa +]Ilm ₉₈ + Mag ₃₁ + F ₄₅

The calculated stability field of quartz + magnetite + graphite

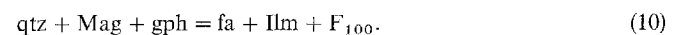
Interpretation of Fig. 8 does not involve any principles that are not already familiar to petrologists through $T-X_{\text{CO}_2}$ diagrams. However, because $P-T$ projections for systems with a fluid of variable composition are not widely used, it may be helpful to consider the stability field of $\text{qtz} + \text{mag} + \text{F}$ [+ gph]⁴ in the C–O–H–FeO–SiO₂ system as an aid to understanding the utility of the $P-T$ projection and its relation to $T-X_{\text{O}}$ diagrams. In Fig. 8a it is seen that the lower $T-X_{\text{O}}$ limit for $\text{qtz} + \text{mag}$ [+ gph] is the isobaric invariant point P₄₅, that is simultaneously the upper limit for $\text{gru} + \text{sid}$ (the $\text{gru} + \text{sid}$ field is extremely narrow below P₄₅ in Fig. 8a), it follows that this isobaric invariant point locates the conditions for the univariant $P-T$ equilibrium $\text{gru} + \text{sid} = \text{qtz} + \text{mag} \pm \text{F}$ [+ gph], i.e., the curve extending from P₂₄ to invariant point P₂₅ in Fig. 9a. For the specific conditions of Fig. 8a, the quantitative stoichiometry of the equilibrium reaction is:



The effect of pressure on this equilibrium is to shift the fluid composition from $X_{\text{O}} = 0.36$ to $X_{\text{O}} = 0.43$ with

increasing pressure (points P₂₄ and P₂₅), which causes the stoichiometry to vary accordingly. A counterintuitive implication of Eq. 9 is that prograde devolatilization of the divariant assemblage $\text{sid} + \text{gru} + \text{qtz} + \text{mag} + \text{C-O-H}$ fluid would buffer fluid composition toward conditions for graphite precipitation, i.e., those for Eq. 9. The high temperature limit of $\text{qtz} + \text{mag}$ is defined in Fig. 8a by the extremum point P₄₆, which corresponds to the singular curve $\text{qtz} + \text{mag}$ [+ gph] = $\text{fa} + \text{F}_{100}$ in Fig. 9a that terminates at invariant point P₄₄. At pressures above this invariant point, the high temperature limit of $\text{qtz} + \text{mag}$ in $T-X_{\text{O}}$ diagrams becomes restricted to progressively more water-rich compositions by the $\text{qtz} + \text{mag} + \text{sid} + \text{fa}$ invariant point (P₄₉, Fig. 8b). In $P-T$ projection (Fig. 9a) these invariant points appear as the “fluid-absent” univariant equilibrium $\text{mag} + \text{qtz}$ [+ gph] = $\text{sid} + \text{fa}$ that is only stable in the presence of GCOH fluid between invariant points P₄₄ and P₂₅.

The stability field of qtz (or bqtz) + $\text{Mag} + \text{F}$ [+ gph] in the C–O–H–FeO–TiO₂–SiO₂ system is complicated by solution behavior. The origin of this complication is that, at graphite-saturated conditions, the magnetite-content of Mag decreases more rapidly with temperature than does the hematite-content of Ilm . Thus, at low pressure $\text{qtz} + \text{Mag}$ [+ gph] devolatilizes by the reaction:



The phase field for Eq. 10 has a positive Clapeyron slope at low temperature and pressure (e.g., at point

⁴ Square brackets are used here to denote the participation of phases that are constrained to be present in excess in the phase diagrams of Figs. 8–10.

P_{31} , Fig. 9b), so that with increasing pressure the magnetite-content of Mag decreases. This, in turn, reduces the reaction coefficients of graphite and fluid until they vanish at the graphite- and fluid-absent singular point (P_{32} , Fig. 9b), which is virtually identical with the pressure maximum of equilibrium Eq. 10. At temperatures above this singular point, $fa + Ilm [+ gph]$ becomes the reduced assemblage, and the stability of quartz + Mag is favored with increasing temperature. Consequently, at pressures below the $P-T$ singular point, $T-X_O$ sections for the C-O-H-FeO-TiO₂-SiO₂ system have two separate stability fields for Mag + qtz: a low temperature field for Ti-poor compositions, and a high temperature field for Ti-rich compositions (perhaps more properly designated ulvöspinel). At pressures above the $P-T$ singular point, these fields merge, and the trace of the fluid- and graphite-absent singular curve $bqtz + Mag = fa + Ilm$ (extending from the singular point P_{32} through point P_{42} in Fig. 9b) locates the resulting inflection in the $fa + Ilm = bqtz + Mag$ $T-X_O$ phase field (P_9 , Fig. 8a).

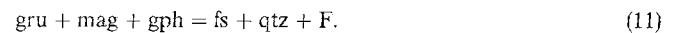
Petrological implications of the C-O-H-FeO-TiO₂-SiO₂ petrogenetic grid

In the analysis of the phase relations of metamorphosed iron-formations it is commonly assumed that solution behaviour stabilizes iron-silicates relative to $qtz + mag$ (e.g., Burt 1972; Frost 1979b; Miyano and Klein 1983). Given this assumption, the C-O-H-FeO-SiO₂ system is an important limiting model for iron-formations, as it defines the maximum stability of $qtz + mag$. Because graphite (or carbonaceous matter), quartz and magnetite are ubiquitous in low and medium grade metamorphosed iron-formations, many authors (e.g. French 1968; Burt 1972) assumed that $qtz + mag$ is stable in the presence of graphite. Subsequent authors rejected this possibility on the basis that it would preclude the stability of $sid + fa$ assemblages (e.g., Bonnicksen 1975; Frost 1979b). This objection is strictly valid only for the C-O-FeO-SiO₂ system, and only if the possible effects of pressure are not considered; thus it cannot be raised in the context of the projection shown in Fig. 8a, that is consistent with Burt's (1972) phase diagram topology at pressures below the $qtz + mag [+ gph] = sid + fa$ univariant field, and with Frost's (1979b) topology at higher pressures. The uncertainty in the pressure ($\hat{S}_p = 1.1$ kbar) of the $qtz + mag [+ gph] = sid + fa$ is relatively small. Therefore, it can be stated with confidence that stability of the $qtz + mag [+ gph]$ assemblage is not a computational artifact.

Although the calculated stability field of $qtz + Mag$ extends to more reduced conditions than inferred by Frost (1979b), neither the $qtz + Mag$ nor siderite fields cross the $X_O = \frac{1}{3}$ boundary for graphite-saturated systems, even at temperatures as low as 300°C. Because

$X_O < \frac{1}{3}$ H-O fluid is more reduced than GCOH fluid of equivalent X_O (Fig. 2b), this implies that $qtz + Mag$ and siderite cannot be stable in $X_O < \frac{1}{3}$ C-O-H fluids. Consequently, the calculated C-O-H-FeO-TiO₂-SiO₂ petrogenetic grid supports the common assumption that the fluid phase during the metamorphism of iron-formations is predominantly an H₂O-CO₂ mixture (e.g., Butler 1969; Frost 1979b; Miyano and Klein 1983). Moreover, as the generation of $X_O < \frac{1}{3}$ fluids by mineral devolatilization requires the prograde formation of carbonates or oxidized minerals, it can be inferred from the restriction of magnetite and siderite stabilities that inorganic devolatilization processes involving common rock-forming minerals in quartz-bearing lithologies are incapable of generating $X_O < \frac{1}{3}$ fluids.

The observation that magnetite and graphite are "incompatible" in $gru + orthopyroxene + qtz$ rocks of the Wabush iron-formation in Quebec (Butler 1969; Frost 1979b) is actually not inconsistent with the existence of a stability field for $qtz + mag + gph$. This is shown by noting that, because fluid in equilibrium with $qtz + mag$ must have an $X_O > \frac{1}{3}$, dehydration of grunerite to orthopyroxene in the presence of $gph + qtz + mag$ must occur by a reaction of the form:



It can be anticipated that devolatilization reactions of this type are associated with major modal variations of the oxides that are reduced, and graphite that is oxidized, during fluid generation. This behavior contrasts with that to be expected during decarbonation-dehydration reactions (e.g., Eq. 10) in which only minor amounts of graphite are required to adjust the carbon-content of the fluid from the H₂O-CO₂ join to the carbon-saturation surface. Equilibrium Eq. 11 is univariant in the C-O-H-FeO-SiO₂ system, where it is metastable and akin to the univariant field $gru + mag [+ gph] = fa + qtz + F$ (P_{23} to P_{25} in Fig. 9a or point P_{48} , Fig. 8a). Thus, the apparent incompatibility of magnetite and graphite may merely reflect variations in bulk composition and the fact that the metamorphic temperature for the assemblages was above that for the equilibrium Eq. 11. This is supported by Butler's (1969) observation that the only other graphitic assemblages in the Wabush formation include siderite. In the C-O-H-Fe-MgO-SiO₂ system, a more appropriate model for the Wabush iron-formation, Eq. 11 becomes divariant, but would still be constrained to occur within the $qtz + mag [+ gph]$ stability field of the C-O-H-Fe-SiO₂ system. In this respect, it is reassuring to observe that Butler's estimate of metamorphic conditions (6 kbar, and 600°C) lies within the calculated field.

The argument here, that $qtz + mag [+ gph]$ is stable in the C-O-H-FeO-SiO₂ system, is not an argument for the importance of this assemblage in

natural systems. Indeed, the restricted P - T field for $\text{qtz} + \text{mag} [+ \text{gph}]$ suggests that the Frost (1979b) is correct in doubting that many of the occurrences of the assemblage represent equilibrium parageneses. Despite this, there are less equivocal examples of natural $\text{qtz} + \text{Mag} + \text{Ilm} + \text{gph}$ parageneses in metapelitic rocks (McLellan 1985; Burton and O'Nions 1991). The metamorphic conditions estimated by McLellan (6 kbar, 500–650°C, $X_{\text{O}} \approx \frac{2}{3}$) and Burton and O'Nions (5 ± 0.5 kbar, $460 \pm 20^\circ\text{C}$, $X_{\text{O}} \approx 0.9$) are in broad agreement with the computed $\text{qtz} + \text{Mag}$ stability field (Fig. 9b). However, the high X_{O} estimates are not consistent with the water-rich conditions required to stabilize $\text{qtz} + \text{mag} [+ \text{gph}]$ with respect to siderite at low temperatures. If these assemblages were, in fact, stable with fluids of the compositions inferred, the stability of siderite must be overestimated in Fig. 9a. This is unlikely given by the rarity of $\text{qtz} + \text{mag} [+ \text{gph}]$ and the small statistical uncertainty for the siderite stability limit ($\hat{s}_T \approx 5^\circ\text{C}$, $\hat{s}_P \approx 200$ bar).

Although the $\text{qtz} + \text{Mag} [+ \text{gph}]$ assemblage may be relatively uncommon, its stability relative to $\text{sid} + \text{fa}$, as defined by the univariant equilibrium $\text{qtz} + \text{Mag} [+ \text{gph}] = \text{sid} + \text{fa}$ is a potential barometer for iron-formations, a lithology notorious for its lack of pressure indicators. The effect of graphite-undersaturation on the C-O-H-FeO-SiO_2 phase fields of Fig. 9a is identical to an increase in f_{O_2} , namely to increase the stability of magnetite-bearing assemblages. Thus, the maximum stability of non-graphitic $\text{sid} + \text{fa}$ assemblages in the presence of fluid in the C-O-H-FeO-SiO_2 system is limited at low temperature by the equilibrium $\text{gru} + \text{mag} [+ \text{gph}] = \text{fa} + \text{sid} + \text{F}$, and at low pressure by the equilibrium $\text{qtz} + \text{Mag} [+ \text{gph}] = \text{sid} + \text{fa}$ (Fig. 9b). An oft cited example of a natural $\text{sid} + \text{fa}$ paragenesis is the assemblage fa ($X_{\text{Fe}} = 0.971$) + sid ($X_{\text{Fe}} = 0.928$) + gru ($X_{\text{Fe}} = 0.97$) + $\text{mag} + \text{qtz}$ from the Gunflint iron-formation described by Floran and Papike (1978, their sample 67–223). If Mg-solution is taken into account with ideal-solution models, the stability field of this assemblage expands in comparison to that shown in Fig. 9a, yielding P - T conditions of 5.8 kbar and 575°C ($X_{\text{O}} = 0.53$) and 5.1 kbar and 615°C ($X_{\text{O}} = 1$) for the activity “corrected” invariant points P_{25} and P_{24} of Fig. 9a. With a generous estimate of the error for the activities of fayalite, siderite, and grunerite (± 0.1 , ± 0.05 , ± 0.35 , respectively), the \hat{s}_P for these points is ca. 2 kbar. If correct, this suggests higher pressures than commonly assumed for the contact metamorphism of the Gunflint iron-formation, and by association for intrusion of the Duluth complex. Although such a statement may seem controversial, most previous pressure estimates (2–4 kbar) have been proposed as minimum estimates (e.g., French 1968; Simmons et al. 1974). A notable exception is the upper limit on metamorphic pressure (2.5 kbar) assessed by Labotka et al. (1981) with sphalerite barometry for the Rove formation,

which is stratigraphically higher than the Gunflint formation.

The $\text{C-O-H-FeO-TiO}_2\text{-SiO}_2$ system phase relations of Figs. 8–10 define the maximum stability, and extent of Ti-solution, for Fe-Ti oxides in graphitic metapelites, with the possible exception of Cr- and Mn-rich lithologies. These phase relations are in agreement with the observation opaque mineralogy of graphitic metapelites as recently reviewed by Frost (1990). Restriction of the $\text{qtz} + \text{Mag}$ field to $X_{\text{O}} > \frac{1}{3}$ fluid compositions, which becomes more pronounced in Mg- and Al-rich systems, is consistent with the rarity of this assemblage. Ilmenite solution is extremely limited at $X_{\text{O}} = \frac{1}{3}$, varying from $\text{Il}_{99.5}$ to Il_{96} over the P - T conditions illustrated in Fig. 9. These compositions are nearly independent of temperature, and become progressively more restricted and ilmenite-rich with decreasing pressure. With increasing X_{O} , the hematite-content of ilmenite is predicted not to exceed 7 mol% (Table 3, Fig. 10). Natural ilmenites from graphitic metapelites often have no significant hematite component (e.g., Scvigny and Ghent 1989; Connolly et al. 1994), while this may reflect water-rich fluid compositions it may also be attributable to retrograde effects. A separate ulvöspinel phase may be stable in quartz-undersaturated systems at temperatures below the critical curve of the Usp-Mag solvus (P_{47} , Fig. 8a; P_{50} – P_{51} , Fig. 9b). The stability of such a phase in natural systems at $P > 2$ kbar would be indicative of $X_{\text{O}} < \frac{1}{3}$ fluids.

Graphite stability diagrams

P - T - X_{O} phase diagrams define the equilibrium conditions for graphite precipitation in response to changes in pressure and temperature, but often it is the evolution of fluid composition in response to fluid-rock disequilibrium that is of interest, as in metasomatic systems. In this case there is no option but to resort to isobaric-isothermal phase diagrams that specify both compositional degrees of freedom of the fluid in a rational manner (Frost 1979a). Because the carbon-saturation surface approaches the O-H join at $X_{\text{O}} = \frac{1}{3}$ there is no single choice of compositional variables that provides comparable graphical resolution for all regions of interest. One solution to this problem is to describe C-O-H fluid composition in terms of displacements relative to $\text{CH}_4\text{-H}_2\text{O}$ and $\text{H}_2\text{O-CO}_2$ joins. As seen in Fig. 1, description relative to the $\text{H}_2\text{O-CO}_2$ join is convenient for $X_{\text{O}} > \frac{1}{3}$ compositions, whereas that relative to the $\text{CH}_4\text{-H}_2\text{O}$ join is preferable at $X_{\text{O}} < \frac{1}{3}$. The selection of the third component necessary to define the ternary composition space in each case is arbitrary; for present purposes the components are chosen as $\text{H}_2\text{O-CO}_2\text{-O}$ and $\text{CH}_4\text{-H}_2\text{O-H}$. Fig. 11 shows the location of the carbon-saturation surface at various P - T conditions in these composition spaces; in

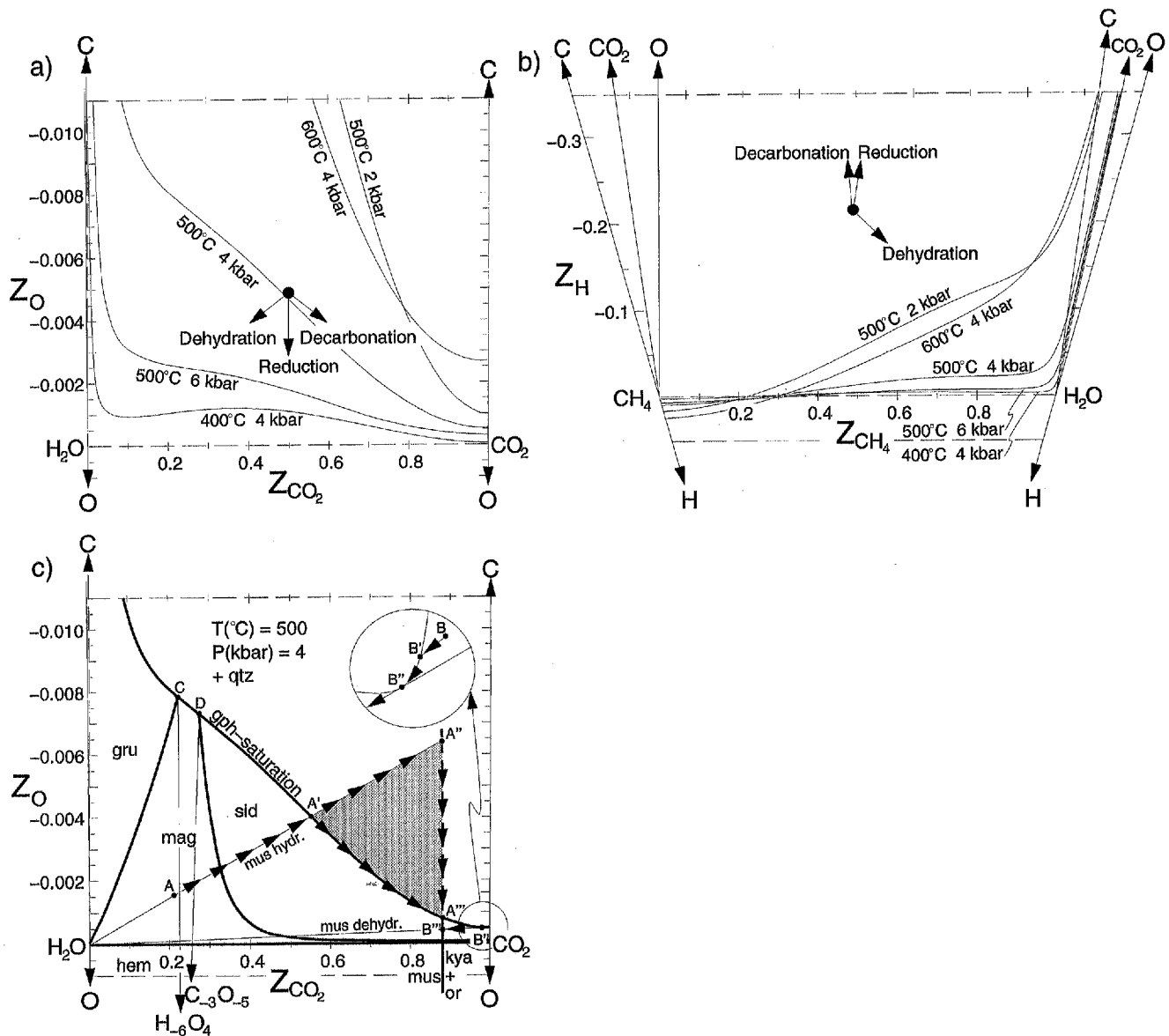


Fig. 11a-c Calculated graphite-saturation surface in composition spaces H₂O-CO₂-O (a) and CH₄-H₂O-H (b). For fluid compositions shown by filled circles in a and b, arrows indicate how mineral devolatilization processes change the compositions. c Calculated isobaric-isothermal univariant fields (heavy solid curves) for the quartz-saturated C-O-H-FeO-SiO₂ and C-O-H-K₂O-Al₂O₃-SiO₂ systems

as a function of fluid composition defined by the components H₂O-CO₂-O. The mag = hem univariant field is essentially coincident with, though slightly above the H₂O-CO₂ join, and the mus = kya + or univariant field is the approximately vertical line at Z_{CO₂} = 0.88, extending to metastable fluid compositions at A". Shaded field and arrows indicate fluid evolution paths discussed in text

both composition spaces $X_O = \frac{1}{3}$ composition corresponds to the C-H₂O tieline, and, in the limit that the fluid composition approaches the CO₂-H₂O and H₂O-CH₄ joins, the component mole fractions Z_{CO₂} and Z_{CH₄} are related to X_O as in Eqs. 6 and 7.

Metasomatic graphite precipitation

The compositional evolution of a metasomatic fluid depends only upon its initial composition and the proportions of the fluid components released or consumed

during equilibration. Thus if the conditions for mineral equilibria are projected onto the fluid composition space, it is a relatively simple matter to determine processes that can lead to graphite precipitation. This is illustrated by Fig. 11c, which shows quartz-saturated equilibria in the C-O-H-FeO-SiO₂ system and the C-O-H-K₂O-Al₂O₃-SiO₂ dehydration equilibrium muscovite (mus) = orthoclase (or) + kyanite (kya). Consider the interaction of a kya + or rock with a fluid of initial composition A in Fig. 11c. Because composition A lies to the water-rich side of the mus = kya + or [+qtz] equilibrium, introduction of the fluid into the

rock results in hydration, depleting the fluid in H_2O . This is the only possible process as long as the fluid remains undersaturated with respect to carbon; thus the composition of the fluid must shift directly away from the H_2O component along the path $A \rightarrow A'$.

Beyond composition A' the possible evolution of the system becomes ambiguous because the relative rates of muscovite formation and graphite precipitation cannot be determined from an equilibrium model. If the rate of graphite precipitation is low, the system may achieve conditions for the metastable $\text{mus} = \text{kya} +$ or $[\text{+qtz}]$ equilibrium at composition A'' , and subsequently evolve toward A''' with graphite precipitation. The concentration of graphite produced by this process is in principle unlimited, in that it is constrained only by the rate at which graphite is ultimately precipitated. However, the change in composition from A to A'' generates an excess carbon content of only $0.00008 \text{ mol C/mol mus}$. Thus, generation of significant quantities, as opposed to concentrations, of graphite by this mechanism at the specified conditions requires massive hydration. Alternatively, if the fluid cannot become carbon-supersaturated, its composition shifts along the saturation surface toward A''' . In the latter case, the amount of graphite precipitated is coupled to the amount of hydration by the slope of the saturation surface. Over the interval $A' \rightarrow A'''$, this slope averages $0.002 \text{ mol C/mol H}_2\text{O}$; hence production of 1 cm^3 muscovite precipitates a minute quantity of graphite, ca. 0.0002 cm^3 .

The principle illustrated by muscovite hydration can be applied to any reaction of known stoichiometry. For example, if magnetite forms by the combined dehydration-oxidation reaction $3 \text{gru} + 7 \text{O} = 7 \text{mag} [\text{+24qtz}] + 3 \text{H}_2\text{O}$, or equivalently $3 \text{gru} + \text{H}_{-6}\text{O}_4 = 7 \text{mag} [\text{+24qtz}]$, fluid composition is driven directly away from the composition of the "species" H_{-6}O_4 ($Z_{\text{O}} = -0.75$, $Z_{\text{H}_2\text{O}} = 1.75$). Given that grunerite can only be in equilibrium with graphite $[\text{+qtz}]$ and fluid of composition C in Fig. 11c, it follows that formation of magnetite by grunerite dehydration can precipitate graphite only if the initial fluid composition lies to the right of the tieline connecting composition C with H_{-6}O_4 . Likewise, siderite decarbonation-oxidation to produce magnetite can only lead to graphite precipitation if the initial fluid is more water-rich than the tieline between composition D and $\text{C}_{-3}\text{O}_{-5}$ (Fig. 11c). In composition to the muscovite hydration reaction, a negligible amount of siderite or grunerite oxidation is necessary to saturate an initial fluid of composition A (Fig. 11c) in carbon. In the case of grunerite, the oxidation of one mole of grunerite to magnetite is sufficient to saturate 376 moles of the initial fluid A. Thereafter, each mole of grunerite oxidized along the saturation surface precipitates one mole of graphite.

It would be incorrect to conclude from this discussion that mineral oxidation reactions are a more effective mechanism of precipitating graphite than are

hydration reactions. The efficacy of a given mechanism is dependent on the direction in which mineral reactions drive fluid composition relative to the carbon-saturation surface. This in turn is dependent on the reaction stoichiometry and the initial fluid composition. Because of the inflection in the carbon-saturation surface near the $X_{\text{O}} = \frac{1}{3}$ composition, both redox and carbonation-decarbonation reactions become ineffective in water-rich fluids, arguably the most common metamorphic fluids, leaving hydration reactions as the only mechanism of metasomatic graphite precipitation. Indeed, muscovite hydration has been shown to be an effective means of precipitating graphite in metapelitic rocks (Hollister and Buruss 1976). At least two additional inflections can occur along the saturation surface in the vicinity of the $\text{CO}_2\text{-H}_2\text{O}$ join (Fig. 11ab). The existence of such inflections makes it possible, although perhaps not probable, for virtually any type of mineral reaction to precipitate graphite from C-O-H fluid. Ordinarily dehydration induced by infiltration of a CO_2 -rich fluid should be incapable of driving graphite precipitation, as its primary effect is to dilute the carbon-content of the fluid. However, as illustrated in Fig. 11c, the existence of an inflection in the carbon-saturation surface at composition B'' , implies that muscovite dehydration driven by a fluid more CO_2 and carbon-rich than B'' may cause graphite precipitation. The path $B \rightarrow B'''$ suggests the possibility of separating the dehydration reaction front (at B''') from the zone of metasomatic graphite ($B' \rightarrow B''$). Such a separation has been observed in graphitic talc-magnesite serpentinites formed by the infiltration of CO_2 from adjacent carbonate-rich metapelites, with no evident associated mineral oxidation (Surour 1993). Thus, while the illustration provided by Fig. 11c may seem improbable, this mechanism does appear to operate in natural environments, where different physical conditions and chemistry may enhance the inflections shown in Fig. 11a. These inflections have different origins. The inflection at water-rich compositions (e.g., 500°C and 6 kbar, 400°C and 4 kbar, Fig. 11a) is due to water non-ideality, which is accentuated at high pressure or low temperature and by electrolytic contaminants. In contrast, the inflection at CO_2 -rich compositions, reflecting the intersection of the carbon-saturation surface with the $\text{CO}_2\text{-H}$ join (see also Fig. 2c), is dampened with decreasing temperature and increasing pressure as the saturation surface approaches the $\text{CO}_2\text{-H}_2\text{O}$ join.

Carbon activity diagrams

Phase diagrams based on true compositional variables offer the only means of unambiguously interpreting metasomatic phase relations of systems in which the compositional degrees of freedom of the fluid are unconstrained. Unfortunately, they do not provide

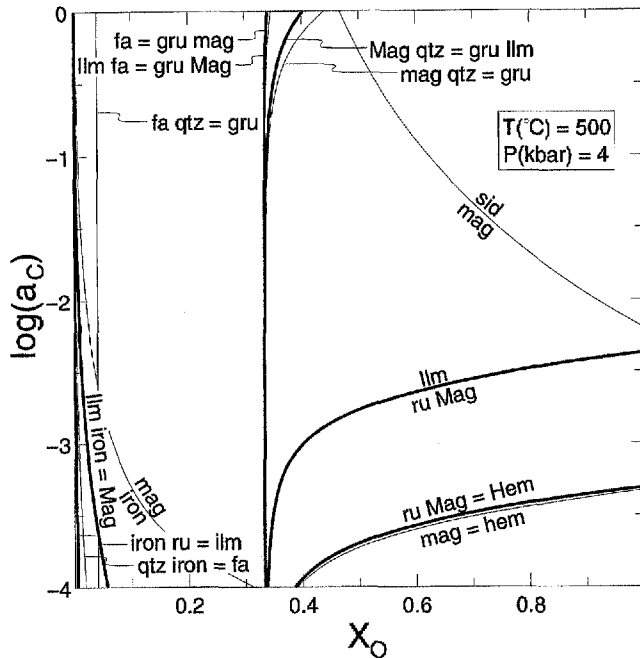


Fig. 12 Calculated isobaric-isothermal $\log a_C$ - X_O phase diagram projection for the C-O-H-FeO-TiO₂-SiO₂ system. Thin curves are C-O-H-FeO-SiO₂ subsystem phase fields. Where reactions are written on a single line, high X_O assemblage is to the right. Equilibria on the carbon-saturation surface ($\log a_C = 0$) correspond to an isothermal section of Fig. 8a

a practical means of representing carbon-undersaturated phase relations more generally because natural C-O-H fluid compositions are largely confined to the narrow region between the carbon-saturation surface and the CH₄-H₂O and H₂O-CO₂ joins. To develop a general method of representing carbon-undersaturated phase relations it is necessary to employ variables that expand this region at the cost of direct physical meaning. Any thermodynamic potential of the fluid components, or derivative quantity (e.g., μ_i , a_i , f_i), well serves this purpose. Thus Frost (1979a) suggested the use of a phase diagram coordinate frame defined by the variables Y_C and $\log f_{O_2}$. An alternative projection, illustrated by Fig. 12 for the fluid-saturated portion of the C-O-H-FeO-TiO₂-SiO₂ system, is defined by the variables X_O and $\log a_C$. For purposes of orientation note that equilibria at $\log a_C = 0$ in Fig. 12 correspond to the equilibria in Fig. 8a at 500°C, and that the activities of carbon along the H₂O-CO₂ join at $X_O = 0.4$ and $X_O = 1$ are ca. $10^{-8.5}$ and $10^{-19.3}$, respectively. The a_C - X_O and f_{O_2} - Y_C diagrams portray the same information and, unless the variables correspond to the independent variables for a process, there is no fundamental reason to prefer one over the other. However, the a_C - X_O projection has the practical advantages of an easily interpreted compositional variable and a simple geometry, in that the graphite-saturation surface corresponds to the $\log a_C = 0$

boundary. Additionally, the X_O location of phase field extrema with respect to the a_C variable is constrained by mass balance in the same manner as in the T - X_O projection; thus, T - X_O and $\log a_C$ - X_O diagrams are topologically equivalent. Extrapolation of Anderson and Lindsley's (1988) model for the R $\bar{3}$ structure, as done here, to hematite-rich compositions leads to underestimation of the stability of ilmenitic hematite. However, even allowing for gross error in the hematite solution model, comparison of Figs. 12 and 11c suggests that hematite-bearing parageneses are diagnostic of binary H₂O-CO₂ fluids, and that any other C-O-H-FeO-TiO₂-SiO₂ paragenesis is indicative of the compositional displacement toward the carbon-saturation surface in $X_O > \frac{1}{3}$ C-O-H fluid.

The a_C - X_O and f_{O_2} - Y_C diagrams have little value for analyzing metasomatic phase relations because of the extremely irregular variation of the potentials a_C and f_{O_2} with fluid composition. This is illustrated by the oxidation-decarbonation of siderite to produce magnetite, $3 \text{ sid} + \text{O} = \text{mag} + 3 \text{ CO}_2$. The oxidation component of this reaction drives the composition of an $X_O > \frac{1}{3}$ fluid toward the carbon-saturation surface (Fig. 11a) increasing both a_C and f_{O_2} , but this is countered by decarbonation that generally lowers both potentials. It is seen in Fig. 11c that oxidation is the dominant effect at 4 kbar and 500°C, but there is no way to determine this with any rigor from Fig. 12. Therefore, although it is evident that siderite decomposition must increase both X_O and Y_C in the fluid, it is not possible to determine whether a_C and f_{O_2} increase or decrease.

Summary and discussion

The composition C-O-H fluid in graphitic rocks is controlled by the proportions of hydrogen and oxygen released or consumed by mineral reactions. As a measure of these proportions X_O directly reflects the mass balance constraints that operate during fluid-rock interaction. Consequently, when it is necessary to consider fluid composition in the analysis of graphitic rocks, X_O is the best possible fluid compositional variable for constructing phase diagrams. From a thermodynamic point of view the speciation of GCOH fluid is irrelevant and, given the carbon-saturation constraint, GCOH fluids can be treated as binary O-H fluids after projection through carbon. A particular benefit of this method is that it facilitates construction and interpretation of phase diagrams in which the complete compositional phase relations of a system are projected onto a P - T coordinate frame. Such projections define the conditions for GCOH fluid generation and the stability of mineral assemblages in both fluid saturated and undersaturated (i.e., either fluid-absent or fluid-underpressured) systems. In graphite-free systems C-O-H fluid is often modeled as a binary H₂O-CO₂ fluid. At

$X_{\text{O}} > \frac{1}{3}$ GCOH fluids closely approximate $\text{H}_2\text{O}-\text{CO}_2$ fluids in terms of major species, but are considerably more reduced. GCOH fluid therefore provides an alternative to the $\text{H}_2\text{O}-\text{CO}_2$ model, in which f_{O_2} is poorly defined, in that X_{O} and X_{CO_2} are simple related and that $P-T-X_{\text{O}}$ diagrams define the maximum stability of reduced phase assemblages.

A simple example of the value of this last feature is provided by the $\text{C}-\text{O}-\text{H}-\text{FeO}-\text{SiO}_2$ system, a model for the phase relations of metamorphosed iron-formations. In this system, the maximum stability of the $\text{sid} + \text{fa}$ assemblage is limited at low pressure by the equilibrium $\text{sid} + \text{fa} = \text{qtz} + \text{mag} + \text{gph}$, a potential geobarometer. The significance of this equilibrium, and its pyroxene equivalent, does not appear to have been recognized earlier because most phase diagrams for the $\text{C}-\text{O}-\text{H}-\text{FeO}-\text{SiO}_2$ system have been constructed assuming the stability of $\text{qtz} + \text{mag}$ at all conditions. The difficulty with this assumption is that it precludes the stability of equilibria in which silicates and/or carbonates breakdown to $\text{qtz} + \text{mag}$ and graphite or a $\text{C}-\text{O}-\text{H}$ -fluid. The calculated stability field of $\text{qtz} + \text{mag} + \text{gph}$ extends to pressures of about 8 kbar and may be slightly underestimated if the conditions inferred by McLellan (1985) and Burton and O'Nions (1991) for the occurrence of this assemblage in metapelites are correct. In any case, this suggests a minimum pressure of 5 kbar ($\hat{S}_P = 2$ kbar) was necessary to stabilize the $\text{sid} + \text{fa}$ assemblage reported by Floran and Papike (1978) in the contact metamorphosed Gunflint iron-formation. Although subject to considerable uncertainty, this implies higher pressures for the emplacement of the Duluth complex than supposed from stratigraphic reconstructions (e.g., French 1968; Pasteris 1988). For most graphitic metapelites, $\text{C}-\text{O}-\text{H}-\text{FeO}-\text{TiO}_2-\text{SiO}_2$ system phase equilibria define the maximum stability of $\text{Fe}-\text{Ti}$ oxides. Calculated $P-T-X_{\text{O}}$ phase diagram projections for the $\text{C}-\text{O}-\text{H}-\text{FeO}-\text{TiO}_2-\text{SiO}_2$ system indicate that in the presence of $\text{C}-\text{O}-\text{H}$ fluid: (i) $\text{qtz} + \text{Mag}$ is only stable at $X_{\text{O}} > \frac{1}{3}$; and (ii) ilmenite solution behavior is virtually independent of $P-T$ conditions in water-rich fluids and is limited to a narrow range of compositions, slightly more hematite-rich (ca. 1–4 mol%) than stoichiometric ilmenite.

Generation of $X_{\text{O}} < \frac{1}{3}$ fluids by inorganic devolatilization reactions requires simultaneous formation of carbonates or relatively oxidized minerals. In quartz-bearing rocks, the restriction of both carbonate and magnetite stability fields to $X_{\text{O}} > \frac{1}{3}$ fluids implies that devolatilization of common rock-forming mineralogies cannot generate $X_{\text{O}} < \frac{1}{3}$ fluid. Although not presented here, calculated $P-T-X_{\text{O}}$ phase equilibria (Connolly 1994) for the $\text{C}-\text{O}-\text{H}-\text{Fe}-\text{MgO}-\text{SiO}_2$ system show that this conclusion holds as well for ultramafic rocks, with the exception of reactions involving brucite and magnesite. At low pressure (< 5 kbar), brucite-magnesite reactions are capable of generating fluids with compositions approaching $X_{\text{O}} \approx 0.1$ ($y_{\text{CH}_4} \approx 64$ mol%).

Whether the kerogen component present in natural graphitic material plays an important role in the generation of $X_{\text{O}} < \frac{1}{3}$ fluids is problematic. The bulk of the transformation from kerogen to graphite appears to occur at low metamorphic grades ($< 300-400^\circ\text{C}$, e.g., French 1968; Buseck and Bo-jur 1986), and consequently would not be expected to contribute an important component to fluids generated at higher grades. However, kerogen has been identified in sillimanite grade metamorphic rocks (e.g., Large et al. 1994), and Rumble and Hoering (1986) inferred from isotopic evidence that $X_{\text{O}} < \frac{1}{3}$ fluids, derived from kerogen decomposition, were responsible for formation of graphite veins in sillimanite grade rocks.

The isobaric-isothermal $X_{\text{O}}-a_{\text{C}}$ phase diagram projection suggested here provides a means of describing phase relations in carbon-undersaturated systems that is similar to the well known $Y_{\text{C}}-f_{\text{O}_2}$ diagram of Frost (1979a). A difficulty in employing such diagrams is that the path defining the locus of fluid compositions resulting from a metasomatic processes cannot be predicted with certainty. There is no universally practical solution to this problem, but the mass balance constraints on fluid evolution become apparent if equilibrium conditions are projected onto the fluid composition space. Through such projections it has been shown that in certain circumstances graphite precipitation can be driven by almost any type of mineral-volatile reaction.

The primary purpose of this paper was to demonstrate that the formalism necessary to treat phase equilibria with GCOH fluids is no more complicated than that for $\text{H}_2\text{O}-\text{CO}_2$ fluids. This is true only in theory, for GCOH fluid equilibration involves both heterogeneous and homogeneous reactions. Innumerable studies have shown that in natural and experimental systems perfect GCOH fluid equilibrium is never realized, but the quantitative importance of disequilibrium cannot be assessed with any rigor. Thus, at present GCOH fluids can only be accepted as a limiting model with the understanding that fluid speciation may be affected by many factors. Aside from the inevitable complications of additional fluid components, two key assumptions in speciation calculations for graphite-saturated systems may be of limited validity in natural systems. These are that carbonaceous matter in metamorphic rocks is perfectly crystalline graphite, and that the fluid present during metamorphism is in equilibrium with this material. As noted above, carbonaceous material in metamorphic rocks is typically neither pure nor well crystallized. It is probable that such material is metastable with respect to perfectly crystalline graphite at all metamorphic conditions; thus fluid in equilibrium with such material will have more carbon-rich compositions, particularly at low X_{O} , than predicted for GCOH fluid. As illustrated indirectly in Fig. 3, order of magnitude variations in graphite activity are necessary to cause significant changes in fluid speciation, but it is pointless to speculate further on the effect of this

without a thermodynamic model for carbon activity in such material. In experimental systems fluid-graphite disequilibrium can occur at temperatures as high as 750°C (e.g., Ziegenbein and Johannes 1980; Morgan et al. 1992). However, carbonaceous films form readily from C–O–H fluid at 400°C through interactions with chemically active mineral surfaces (Tingle and Hochella 1993), and graphite has also been shown to have precipitated from fluid inclusions trapped at $T < 400^\circ\text{C}$ (Pasteris 1988). These latter observations suggest that even at low temperature metastable equilibration of fluid and carbonaceous matter may not be inhibited in natural environments and on geologic time scales.

Acknowledgements This paper is an outgrowth from an earlier project done in collaboration with B. Cesare, and many of the ideas presented here originated from that project. I am indebted to R. Abart, B. Cesare, B.W. Evans, G.B. Skippen, R. Sweeny and an anonymous reviewer for very constructive reviews. In particular, B.W. Evans asked the right questions (although I may not have provided the right answers), and G.B. Skippen prompted and checked the proof in Appendix 2. T.J.B. Holland provided updated thermodynamic data, and corrected my errors in translating these data. R. Abart calculated the f_{O_2} contours shown in Fig. 2c. Discussions with O. Suleimenov and V. Trommsdorff also resulted in improvements to this paper. Financial support for this work was from Swiss National Science Foundation grant 21-36503.93.

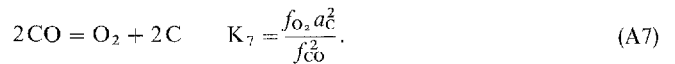
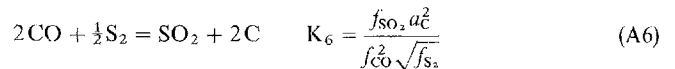
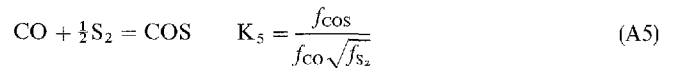
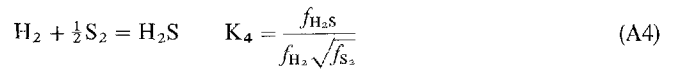
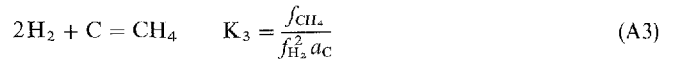
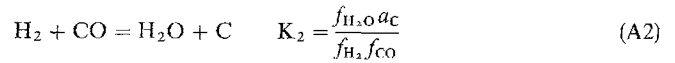
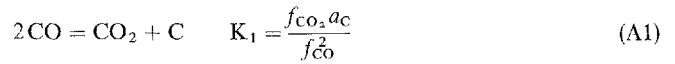
Appendix 1

Calculation of C–O–H–S fluid speciation as a function of X_{O}

Calculation of molecular fluid speciation as a function of a variable that relates the proportions of the fluid components (e.g., X_{O}) involves introduction of additional mass balance constraints that do not appear in calculations as a function of species properties (e.g., French 1966; Eugster and Skippen 1967). To provide a general example of how this is done, the speciation calculation of a C–O–H–S fluid composed of nine significant species (H_2O , H_2S , H_2 , CH_4 , CO_2 , CO , COS , SO_2 and O_2) as a function of X_{O} , a_{C} and f_{S_2} is described here. The formulation for such a fluid can be used to calculate the properties of S-free fluids by lowering f_{S_2} to a value at which sulfur species become negligible; likewise speciation of C-free fluids can be calculated by lowering a_{C} .

In a $c = 4$ component fluid comprised of $n = 9$ species it is possible to write $n - c$ reactions between any set of c species with linearly independent compositions, and each of the remaining species. In the context of the present problem the fugacity, or activity, of $q = 2$ components (C and S_2) are known. To make use of this information it is desirable to write the equilibria in terms of these components. Thus it must be possible to write $n + q - c = 7$ linearly independent reactions between the $n + q = 11$ species and components, each involving, at most, a linearly independent set of $c - q = 2$ species, the set of $q = 2$ constrained components, and one additional species. Equilibrium constants for these reactions can then be used to relate the fugacities, and thereby concentrations, of the $n + q - c = 7$ species to the fugacities of the remaining $c - q = 2$ species and the q constrained components. The choice of the set of $c - q = 2$ species is arbitrary, and is taken as $\{\text{CO}, \text{H}_2\}$ here. The $n + q - c = 7$ reactions and equilibrium constants are

then:



The equilibrium constants are calculated at the P – T condition of interest from tabulations of thermodynamic data such as those provided by Reid et al. (1987). The fugacity of each species can be expressed:

$$f_i = \delta_i \gamma_i \quad (\text{A8})$$

where $\delta_i = f_i^\circ \gamma_i$, f_i° is the fugacity of a pure fluid of the i^{th} species, and γ_i is the activity coefficient of the species in the mixed-volatile fluid. The advantage of separating fluid properties into two terms, f_i° and γ_i , is that any desired equation of state can be used for the pure species. The resulting fugacities can then be combined with activity coefficients from an equation of state that provides appropriate mixing rules, such as the Modified Redlich-Kwong (Holloway 1977).

By rearranging the equilibrium constant expressions Eqs. A1–A7, in combination with Eq. A8 the mole fractions of CO_2 , H_2O , CH_4 , H_2S , COS , SO_2 and O_2 can be written in terms of y_{CO} and y_{H_2} :

$$y_{\text{CO}_2} = C_1 y_{\text{CO}}^2 \quad C_1 = \frac{K_1 \delta_{\text{CO}}^2}{\delta_{\text{CO}_2} a_{\text{C}}} \quad (\text{A9})$$

$$y_{\text{H}_2\text{O}} = C_2 y_{\text{H}_2} y_{\text{CO}} \quad C_2 = \frac{K_2 \delta_{\text{H}_2} \delta_{\text{CO}}}{\delta_{\text{H}_2\text{O}} a_{\text{C}}} \quad (\text{A10})$$

$$y_{\text{CH}_4} = C_3 y_{\text{H}_2}^2 \quad C_3 = \frac{K_3 \delta_{\text{H}_2}^2 a_{\text{C}}}{\delta_{\text{CH}_4}} \quad (\text{A11})$$

$$y_{\text{H}_2\text{S}} = C_4 y_{\text{H}_2} \quad C_4 = \frac{K_4 \delta_{\text{H}_2} \sqrt{f_{\text{S}_2}}}{\delta_{\text{H}_2\text{S}}} \quad (\text{A12})$$

$$y_{\text{COS}} = C_5 y_{\text{CO}} \quad C_5 = \frac{K_5 \delta_{\text{CO}} \sqrt{f_{\text{S}_2}}}{\delta_{\text{COS}}} \quad (\text{A13})$$

$$y_{\text{SO}_2} = C_6 y_{\text{CO}}^2 \quad C_6 = \frac{K_6 \delta_{\text{CO}}^2 \sqrt{f_{\text{S}_2}}}{\delta_{\text{SO}_2} a_{\text{C}}} \quad (\text{A14})$$

$$y_{\text{O}_2} = C_7 y_{\text{CO}}^2 \quad C_7 = \frac{K_7 \delta_{\text{CO}}^2}{\delta_{\text{O}_2} a_{\text{C}}^2} \quad (\text{A15})$$

The mass balance constraint:

$$1 = \sum_{i=1}^n y_i \quad (\text{A16})$$

can be rearranged using Eqs. A9–A15 as a quadratic in y_{CO} :

$$0 = a y_{\text{CO}}^2 + b y_{\text{CO}} + c, \quad (\text{A17})$$

where:

$$a = C_6 + C_1 + C_7 \quad (\text{A18})$$

$$b = 1 + C_5 + C_2 y_{\text{H}_2}, \quad (\text{A19})$$

$$c = C_3 y_{\text{H}_2}^2 + y_{\text{H}_2}(C_4 + 1) - 1. \quad (\text{A20})$$

By experience it is found that the root:

$$y_{\text{CO}} = \frac{-b + \sqrt{b^2 - 4ac}}{2a} \quad (\text{A21})$$

of Eq. A17 is physically meaningful. Through Eqs. A9–A15 and A21, the abundances of all fluid species are expressed solely as a function of y_{H_2} . The value of y_{H_2} may then be determined by employing the mass balance constraint implicit by specification of X_{O} . For algebraic purposes it is simpler to convert this constraint to one on the atomic O:H ratio:

$$\frac{n_{\text{O}}}{n_{\text{H}}} = \frac{X_{\text{O}}}{X_{\text{O}} - 1} \quad (\text{A22})$$

where

$$n_{\text{O}} = 2(y_{\text{O}_2} + y_{\text{CO}_2} + y_{\text{SO}_2}) + y_{\text{H}_2\text{O}} + y_{\text{CO}} + y_{\text{COS}}$$

$$n_{\text{H}} = 2(y_{\text{H}_2\text{O}} + y_{\text{H}_2\text{S}} + y_{\text{H}_2} + 2y_{\text{CH}_4}).$$

Eq. A22 can thus be written as:

$$\frac{n_{\text{O}}}{n_{\text{H}}} = \frac{2C_6 y_{\text{CO}}^2 + y_{\text{CO}} + 2C_1 y_{\text{CO}}^2 + C_2 y_{\text{CO}} y_{\text{H}_2} + C_5 y_{\text{CO}} + 2C_7 y_{\text{CO}}^2}{2C_2 y_{\text{CO}} y_{\text{H}_2} + 2y_{\text{H}_2} + 2C_4 y_{\text{H}_2} + 4C_3 y_{\text{H}_2}^2} \quad (\text{A23})$$

where y_{CO} is an explicit function of y_{H_2} given by Eq. A21.

In practice, the speciation is determined in an iterative procedure consisting of three steps, (i) Equilibrium constants (K_1 – K_7) and fugacities of the pure species fluids are determined at the P – T condition of interest from equations of state. Species activity coefficients are set to unity, and an initial estimate for y_{H_2} is computed subject to the constraint that Eq. A21 must be greater than zero. (ii) Eq. A23, with Eq. A21 substituted for y_{CO} , is solved for y_{H_2} by a numerical method such as Newton-Raphson Iteration. Abundances of the remaining species are computed from Eqs. A9–A15 and A21, and the species activity coefficients are computed from a mixed-volatile equation of state. (iii) The revised estimate of y_{H_2} is compared to the previous value, if the estimates do not differ within a specified tolerance the speciation is accepted. Otherwise step (ii) is repeated.

Graphite-undersaturated C–O–H–S fluids

In treating graphite-free rocks carbon activity is not a meaningful quantitative variable because it varies in an irregular manner within the fluid composition space and because it is not easily quantified from mineral equilibria. In cases where $\bar{G}_{\text{H}_2\text{O}}$, \bar{G}_{O_2} or \bar{G}_{CO_2} (or

equivalently the corresponding fugacity) is constrained by mineral equilibria these constraints can be coupled with Eq. A23 for speciation calculations. This coupling requires replacement of the fluid phase equilibria in Eqs. A1–A7 by a set of $n + q (= 1) - c = 6$ equilibria that do not include a carbon component and introduction of the constraint for the species of known \bar{G}_i :

$$y_i = \left[\frac{\bar{G}_i - G_i^0}{RT \ln \delta_i} \right] \quad (\text{A24})$$

When such constraints cannot be implemented a second possibility is to introduce additional mass balance constraints on the fluid bulk composition. Specification of C:S ratio, Y_{C} or X_{S} are examples of such constraints that have been implemented by the author. Implementation of these constraints involves the solution of an additional equation of the form of Eq. A23, and this requires a doubly iterative solution algorithm. FORTRAN computer programs based on these algorithms, as well as the C–O–H–S speciation algorithm discussed above, are available upon request from the author (please supply a 3.5" Sun, DOS, or MacIntosh disk).

Appendix 2

Conditions for a maximum in thermodynamic activity

The thermodynamic activity or fugacity of a species is directly proportional to its partial molar Gibbs energy. Consequently, the isobaric-isothermal conditions for a maximum in the partial molar Gibbs energy are also the conditions for maxima in activity and fugacity. If a phase exhibits immiscibility, then the partial molar Gibbs energy of any component in the fluid has, at least, a local maximum at the immiscible composition. This case is trivial; the more general case considered here is the identification of the stable, miscible, composition of a phase at which the partial molar Gibbs energy of a given species is maximized. The differential of the partial molar Gibbs energy (\bar{G}_j , Eq. 2) of a species j with stoichiometry $\{v_1^j \dots v_c^j\}$ in a c -component phase is:

$$d\bar{G}_j = \sum_{k=1}^c v_k^j d\mu_k. \quad (\text{B1})$$

The differential $d\mu_c$ can be expressed in terms of the remaining chemical potentials through the Gibbs–Duhem relation:

$$d\mu_c = - \sum_{k=1}^{c-1} \frac{n_k}{n_c} d\mu_k. \quad (\text{B2})$$

Substitution of Eq. B2 into Eq. B1 yields:

$$d\bar{G}_j = \sum_{k=1}^{c-1} \left[v_k^j - v_c^j \frac{n_k}{n_c} \right] d\mu_k. \quad (\text{B3})$$

The partial molar Gibbs energy is therefore a function in $c - 1$ independent variables; the conditions for an extremum in this function are:

$$\left\{ \frac{\partial \bar{G}_j}{\partial \mu_k} = v_k^j - v_c^j \frac{n_k}{n_c} = 0 \right\} \quad k = 1 \dots c - 1, \quad (\text{B4})$$

or equivalently:

$$\left\{ \frac{v_k^j}{v_c^j} = \frac{n_k}{n_c} \right\} \quad k = 1 \dots c - 1. \quad (\text{B5})$$

Thus, the partial molar Gibbs energy of a species can only have an extremum when the species and phase have identical compositions.

To demonstrate that this extremum is a maximum it is convenient to introduce a set of normal equations in $\{n_1 \dots n_{c-1}\}$ from Eq. B3:

$$\left\{ \frac{\partial \bar{G}_j}{\partial n_h} = \sum_{k=1}^{c-1} \left[v_k^j - v_c^j \frac{n_k}{n_c} \right] \frac{\partial \mu_j}{\partial n_h} \right\} \quad h = 1 \dots c - 1. \quad (\text{B6})$$

The conditions:

$$\left\{ \frac{\partial \bar{G}_j}{\partial n_h} = 0 \right\} \quad h = 1 \dots c - 1. \quad (\text{B7})$$

provide an alternative set of necessary and sufficient conditions for an extremum in \bar{G}_j . From Eq. B4, it follows that these conditions are only satisfied at the phase composition $\left\{ \frac{v_1^j}{v_c^j} \dots \frac{v_{c-1}^j}{v_c^j} \right\}$. For these conditions to be those of a maxima in \bar{G}_j it is sufficient that:

$$\left\{ \frac{\partial^2 \bar{G}_j}{\partial n_k^2} > 0 \right\} \quad k = 1 \dots c - 1. \quad (\text{B8})$$

Partial differentiation of Eq. B6 with respect to $\{n_1 \dots n_{c-1}\}$ yields:

$$\left\{ \frac{\partial^2 \bar{G}_j}{\partial n_h^2} = \sum_{k=1}^{c-1} \left[-\frac{1}{n_c} \left[\frac{\partial n_k}{\partial n_h} \right] \left[\frac{\partial \mu_k}{\partial n_h} \right] + \left[v_k^j - v_c^j \frac{n_k}{n_c} \right] \left[\frac{\partial^2 \mu_k}{\partial n_h^2} \right] \right\} \quad h = 1 \dots c - 1. \quad (\text{B9})$$

For $k \neq h$ the first term of the summation in Eq. B4 vanishes; and, at an extremum, by Eq. B9, the second term in the summation is zero. Thus, at the composition $\left\{ \frac{v_1^j}{v_c^j} \dots \frac{v_{c-1}^j}{v_c^j} \right\}$,

$$\left\{ \frac{\partial^2 \bar{G}_j}{\partial n_h^2} = -\frac{1}{n_c} \left(\frac{\partial \mu_h}{\partial n_h} \right) \right\} \quad h = 1 \dots c - 1. \quad (\text{B10})$$

By making use of the definition of chemical potential:

$$\mu_j \equiv \frac{\partial G}{\partial n_j}, \quad (\text{B11})$$

Eq. B10 can be rewritten as

$$\left\{ \frac{\partial^2 \bar{G}_j}{\partial n_h^2} = -\frac{1}{n_c} \left(\frac{\partial^2 G}{\partial n_h^2} \right) \right\} \quad h = 1 \dots c - 1. \quad (\text{B12})$$

For any stable composition of a phase it follows from Gibbs' stability criterion that:

$$\left(\frac{\partial^2 G}{\partial n_h^2} \right) > 0 \quad (\text{B13})$$

Therefore $\frac{\partial^2 \bar{G}_j}{\partial n_h^2}$ must be negative at the composition $\left\{ \frac{v_1^j}{v_c^j} \dots \frac{v_{c-1}^j}{v_c^j} \right\}$ and the partial molar Gibbs energy must be a maximum.

Conditions for maximum \bar{G}_j in a section at constant μ

The foregoing proof defines the conditions for a isobaric-isothermal global maximum in \bar{G}_j , but in many situations it is of interest to determine the conditions for a maximum in \bar{G}_j at constant chemical potential of one or more components (e.g., along the carbon-saturation surface in the C-O-H system). This is readily

shown by noting that in a system in which s chemical potentials are fixed, Eq. B3 becomes:

$$d\mu_{c-s} = - \sum_{k=1}^{c-s-1} \frac{n_k}{n_{c-s}} d\mu_k. \quad (\text{B14})$$

The same logic applied previously in the general case, can then be applied to demonstrate that the partial molar Gibbs energy of a species has a maximum at the composition:

$$\left\{ \frac{v_k^j}{v_{c-s}^j} = \frac{n_k}{n_{c-s}} \right\} \quad k = 1 \dots c - s - 1, \quad (\text{B15})$$

i.e., when the proportions of the unconstrained components in the phase and species are identical.

Extrema in univariant phase fields as a function of a phase composition

A useful application of the compositional constraint on the maximum of the activity of a species, is that it also determines the compositional coordinate of the possible extrema in univariant phase fields as a function of the composition of a phase and an additional potential variable (P , T , μ , etc.). As a relevant example, consider the devolatilization reaction:



where A is a condensed phase that decomposes to form the condensed phase B and a C-O-H fluid. This reaction can be written equivalently as:



where $C_{v_c} O_{v_o} H_{v_H}$ is a C-O-H "species". From Eq. B15 it follows that this species has its maximum thermodynamic activity in a carbon-saturated fluid when:

$$X_O = \frac{v_o}{v_o + v_H}. \quad (\text{B18})$$

Thus, the univariant equilibrium $A = B$ must have extrema, maxima and/or minima, at this fluid composition in $T-X_O$ or $P-X_O$ diagram sections. It is to be emphasized that the $C_{v_c} O_{v_o} H_{v_H}$ species is no less real or stable, than any other possible species. Indeed, such distinctions are meaningless when applied to species within a phase; however, it is possible to distinguish significant and insignificant species in terms of concentration. In this respect, the real concentration of the species $C_{v_c} O_{v_o} H_{v_H}$ may be vanishingly small, and therefore insignificant.

References

- Abart R, Connolly JAD, Trommsdorff V (1992) Singular point analysis: construction of Schreinemakers projections for systems with a binary solution. *Am J Sci* 292:778-805
- Anderson DJ, Lindsley DH (1988) Internally consistent solution models for Fe-Mg-Mn-Ti oxides. *Am Mineral* 73:714-726
- Bonnichsen B (1975) Geology of the Biwabik Iron Formation, Dunka River area, Minnesota. *Econ Geol* 70:319-340
- Burt DM (1972) The system Fe-Si-C-O-H: a model for metamorphosed iron formations. *Carnegie Inst Washington Yearb* 71:435-443.

- Burton KW, O'Nions KK (1991) High resolution garnet chronometry and the rates of metamorphic processes. *Earth Planet Sci Lett* 107:649–671
- Buseck PR, Bo-Jun H (1985) Conversion of carbonaceous material to graphite during metamorphism. *Geochim Cosmochim Acta* 49:2003–2016
- Butler PM (1969) Mineral compositions and equilibria in metamorphosed iron-formation of the Gagnon region, Quebec, Canada. *J Petrol* 10:56–101
- Connolly JAD (1990) Calculation of multivariable phase diagrams: an algorithm based on generalized thermodynamics. *Am J Sci* 290:666–718
- Connolly JAD (1994) Phase diagrams for graphitic rocks. In: Funicello R, Ricci CA, Trommsdorff V (eds) Phase diagram applications in earth materials sciences, VII Summer School Proceedings. University of Siena, Siena, pp 128–156
- Connolly JAD, Cesare B (1993) C–O–H–S fluid composition and oxygen fugacity in graphitic metapelites. *J Metamorphic Geol* 11:379–388
- Connolly JAD, Trommsdorff V (1991) Petrogenetic grids for meta-carbonate rocks: pressure–temperature phase-diagram projection for mixed-volatile systems. *Contrib Mineral Petrol* 108:93–105
- Connolly JAD, Memmi I, Trommsdorff V, Francheschelli M, Ricci CA (1994) Forward modeling of calcisilicate microinclusions and fluid evolution in a graphitic metapelite (NE Sardinia). *Am Mineral* 79:960–972
- Edwards RL, Essene EJ (1988) Pressure, temperature and C–O–H fluid fugacities across the amphibolite-granulite transition, NW Adirondack Mountains, NY. *J Petrol* 29:39–72
- Eugster HP, Skippen GB (1967) Igneous and metamorphic reactions involving gas equilibria. In: Abelson PH (ed) *Researches in Geochemistry*, Wiley, New York, pp 492–520
- Floran RJ, Papike JJ (1978) Mineral and petrology of the Gunflint Iron-formation, Minnesota-Ontario: correlation of compositional and assemblage variations at low to moderate grade. *J Petrol* 19:215–288
- French BM (1966) Some geological implications of equilibrium between graphite and a C–H–O gas at high temperatures. *Geophys Res* 4:223–253
- French BM (1968) Progressive contact metamorphism at the Biwabik Iron Formation, Mesabi Range, Minnesota. *Minn Geol Surv Bull* 45:1–103
- Frost BR (1979a) Mineral equilibria involving mixed volatiles in a C–O–H fluid phase: the stabilities of graphite and siderite. *Am J Sci* 279:1033–1059
- Frost BR (1979b) Metamorphism of iron-formations: paragenesis in the system Fe–Si–C–O–H. *Econ Geol* 74:775–785
- Frost BR (1990) Stability of oxide minerals in metamorphic rocks. In: Lindsley DH (ed) *Oxide minerals: petrologic and magnetic significance*. (Reviews in Mineralogy Vol. 25) Mineralogical Society of America, Washington DC, pp 569–487
- Greenwood HJ (1962) Metamorphic reactions involving two volatile components. *Carnegie Inst Washington Ann Rep Director Geophys Lab* 61:82–85
- Holland TJB, Powell R (1990) An enlarged and updated internally consistent dataset with uncertainties and correlations: the system K_2O – Na_2O – CaO – MgO – Mn – FeO – Fe_2O_3 – Al_2O_3 – TiO_2 – SiO_2 – C – H_2 – O_2 . *J Metamorphic Geol* 8:89–124
- Hollister L, Buruss RC (1976) Phase equilibria in fluid inclusions from the Khtada Lake metamorphic complex. *Geochim Cosmochim Acta* 40:163–176
- Holloway JR (1977) Fugacity and activity of molecular species in supercritical fluids. In: Fraser D (ed) *Thermodynamics in geology* Reidel, Boston, pp. 161–181
- Large DJ, Christy AG, Fallick AE (1994) Poorly crystalline carbonaceous matter in high grade metasediments: implications for graphitisation and metamorphic fluid compositions. *Contrib Mineral Petrol* 116:108–226
- Labotka TC (1981) Petrology of contact metamorphosed argillite from the Rove Formation, Gunflint Trail, Minnesota. *Am Mineral* 66:70–86
- Labotka TC (1991) Chemical and Physical properties of fluids. In: Kerrick D (ed) *Contact metamorphism (Reviews in Mineralogy vol. 26)*. Mineralogical Society of America, Washington DC, pp 43–104
- Lattard D, Evans BW (1992) New experiments on the stability of grunerite. *Fur J Mineral* 4:219–238
- McLellan E (1985) Metamorphic reactions in the kyanite and sillimanite zones of the Barrovian type area. *J Petrol* 26:789–818
- Miyano T, Klein C (1983) Fluid behavior and phase relations in the system Fe–Mg–Si–C–O–H: application to high grade metamorphism of iron-formations. *Am J Sci* 286:540–575
- Morgan GB, Chou I-M, Pasteris JD (1992) Speciation in experimental C–O–H fluids produced by the thermal dissociation of oxalic acid dihydrate. *Geochim Cosmochim Acta* 56: 281–294
- Ohmoto H, Kerrick DM (1977) Devolatilization equilibria in graphitic schists. *Am J Sci* 277:1013–1044
- Pasteris JD (1988) Secondary graphitization in mantle-derived rocks. *Geology* 16:804–807
- Reid RC, Prausnitz JM, Poling BE (1987) *The properties of gases and liquids*. McGraw-Hill, New York
- Rumble D, Hoering TC (1986) Carbon isotope geochemistry of graphite vein deposits from New Hampshire, U.S.A. *Geochim Cosmochim Acta* 50:1239–1247
- Sevigny JH, Ghent ED (1989) Pressure, temperature and fluid composition during amphibolite facies metamorphism of graphitic metapelites, Howard Ridge, British Columbia. *J Metamorphic Geol* 7:497–505
- Simmons EC, Lindsley DH, Papike JJ (1974) Phase relations and crystallization sequence in a contact metamorphosed rock from the Gunflint Iron-formation, Minnesota. *J Petrol* 15:539–565
- Skippen GB, Marshall DD (1991) The metamorphism of granulites and devolatilization of the lithosphere. *Can Mineral* 29:693–705.
- Surour AA (1993) The petrology, geochemistry and mineralization of some ultramafic rocks, Egypt. PhD thesis, Cairo University
- Thompson AB (1983) Fluid absent metamorphism. *J Geol Soc London* 140:533–547
- Tingle TN, Hochella MF (1993) Formation of reduced carbonaceous matter in basalts and xenoliths: reaction of C–O–H gases on olivine crack surfaces. *Geochim Cosmochim Acta* 57:3245–3249
- Whalen JB, Chappell BW (1988) Opaque mineralogy and mafic chemistry of I- and S-type granites of the Lachlan fold belts, southeast Australia. *Am Mineral* 73:281–296
- Ziegenbein D, Johannes W (1980) Graphite COH fluids: an unsuitable compound to buffer fluid composition at temperatures up to 700°C. *Neues Jahrb Miner monatsch* (7):289–305